Soft Matter

Bridging the Crystal and Solution Structure of a Series of Lipid-Inspired Ionic Liquids

Journal:	*Soft Matter*
Manuscript ID	SM-ART-11-2022-001478.R1
Article Type:	Paper
Date Submitted by the Author:	16-Dec-2022
Complete List of Authors:	Bellia, Sophia; Ave Maria University Huynh, Marissa; Stockton University, Chemistry Program Metzler, Matthew; Stockton University, Chemistry Program Zeller, Matthias; Purdue University, Department of Chemistry Mirjafari, Arsalan; SUNY Oswego Cohn, Pamela; Stockton University, Chemistry Program Hillesheim, Patrick C; Ave Maria University

Bridging the Crystal and Solution Structure of a Series of Lipid-Inspired Ionic Liquids

Sophia A. Bellia,[a] Matthew Metzler,[b] Marissa Huynh,[b] Matthias Zeller,[c] Arsalan Mirjafari,*[,d] Pamela Cohn,*[,b] Patrick C. Hillesheim*[,a]

[a] Department of Chemistry and Physics, Ave Maria University, Ave Maria, Florida, 34142, United States

[b] Chemistry Program, Stockton University, Galloway, New Jersey, 08205, United States

[c] Department of Chemistry, Purdue University, West Lafayette, Indiana, 47907, United States

[d] Department of Chemistry, State University of New York at Oswego, Oswego, New York 13126, United States

Keywords

Hirshfeld surfaces; structural analysis; ionic liquids; crystal structure; solution structure

***Corresponding authors:**
Patrick.Hillesheim@avemaria.edu (P.C.H.)
Pamela.Cohn@stockton.edu (P.C.)
Arsalan.Mirjafari@oswego.edu (A.M.)

Abstract

A series of 1,2-dimethylimidazolium ionic liquids bearing a hexadecyl alkyl chain are thoroughly examined *via* X-ray crystallography. The crystal structures reveal several key variations in the non-covalent interactions in the lipid-like salts. Specifically, distinct cation-cation π interactions are observed when comparing the bromide and iodide structures. Changing the anion to bis(trifluoromethane)sulfonimide (Tf_2N^-) changes these cation-cation π interactions with anion···π interactions. Additionally, several well-defined geometries of the cations are noted based on torsion and core-plane angles of the alkyl chains. Hirshfeld surface analysis is used to distinguish the interactions and geometries in the solid state, helping to reveal characteristic structural fingerprints for the compounds. The solid-state structures of the ionic liquids are correlated with the solution-state structures through UV-vis spectroscopic studies, further emphasizing the importance of the π interactions in the formation of aggregates. Finally, we investigated the thermal properties of the ionic liquids, revealing complex phase transitions for the iodide-containing species. These phase transitions are further rationalized *via* the analysis of the data gathered from the structures of the other crystallized salts.

1. Introduction

Ionic liquids (ILs) are a class of soft materials typically comprised of structurally tailored organic cations and anions.[1] In recent years, ILs have seen prolific growth related to applications of these materials.[2,3] One reason for this growth is that ILs offer the benefit of being highly modular, having numerous points on both the cation and anion that can be synthetically modified to affect a desired change in the properties of the formed materials. Advances in their development have transitioned them from the first generation, where they were merely considered as solvents/media, to a second generation of task-specific ILs where functionalization of the cation, anion, or both provides definite physicochemical properties designed to accomplish a specific task.

Of particular note, increasing the length of the alkyl chains can, to an extent, lower the melting point of the IL.[4] However, the trend of side chain length versus melting point is not linear. It was observed for several homologous series of *N*-alkyl-*N'*-methylimidazolium and quaternary ammonium salts that as the size of the *n*-alkyl chain is increased above approximately nine carbons, the melting points being to rise sharply, resulting in species that are room temperature solids.[5] It should be stated, however, that this trend is not all-encompassing, with subtle changes in either cation or anion structure significantly impacting the physicochemical properties of the materials.[6,7]

While shorter chained ILs tend to be highly sought after compounds due to their lower melting points and viscosity, numerous applications exist wherein longer alkyl chain ILs are more desirable. In particular, long-chain ILs have found numerous applications in liquid crystalline display technology,[8,9] as phase transfer catalysts,[10] lubricants,[11] and as surfactants.[12] ILs with longer alkyl chains have garnered particular interest in their use for biological applications.[13] For example, 1-hexadecyl-3-methylimidazolium chloride (or $[C_{16}C_1im][Cl]$) was found to be a strong inhibitor of drug-resistant yeast, speculatively due to the amphiphilic nature of the salts.[14] Further, ammonium-based ILs bearing a docosyl (C_{22}) chain were used in the fabrication of electrodes for use as sensors for nitrites.[15]

As mentioned, ILs are highly modular. Modification of the alkyl chains via sterics[16] or electronics[17] (or both) readily influences the fluidity and crystallinity of the compounds. For example, incorporating a sulfur atom into aliphatic side chains grafted onto imidazolium cations considerably reduces the liquefaction temperatures of ILs relative to congeners bearing fully saturated side chains of equal length.[18] This effect is in part due to the change in torsion angles of the alkyl chains due to the incorporation of the sulfur moiety. Oxygen containing alkyl chains (i.e., ether moieties), were shown to influence thermal properties of ILs via repulsive O···O interactions in the alkyl chains observed in their crystal structures.[19]

Indeed, knowing the structures and interactions of ILs is critical for understanding the properties and function of these materials.[4,20–22] Analysis of the crystal structures of ILs can offer a wealth of knowledge, in particular with regards to cation-cation, cation-anion, and anion-anion interactions.[23–25] Evaluation and quantification of the non-covalent interactions in ILs promotes the development of models useful in the prediction of novel materials.[5,6] Studies on single crystals of long-alkyl chain bearing ILs is particularly challenging, however, given the difficulties in crystal growth coupled with the complex thermal behavior of the molecules.[26] Specifically, long-alkyl chains tend to disrupt, or at least weaken, lattice formation due to many accessible conformations and geometries of the chains, slowing phase transitions such as crystallization.[23,27] Further, slow crystallization kinetics also play a role in the difficulties with single-crystal formation of these class of ILs. Despite these challenges, however, crystallography has played a key role in the development of this field.

A study by the Hardacre group used small-angle X-ray scattering to elucidate the structures of several long-chain ILs, identifying several key phases and phase-transitions of these imidazolium-based ILs.[28] However, as discussed in their work, single-crystal studies would be needed to properly identify and confirm portions of their studies.

Soon after, the same group reported the single-crystal structures of four 1-methylimidazolium (mim) and 1,2-dimethylimidazolium (dmim) halide salts with C_{14} and C_{18} saturated alkyl side chains.[29] The single-crystal studies confirmed several of the previous results from the small-angle scattering studies as well as correlated structural features to thermal properties. Notably, several unique arrangements of the chains were observed in the solid-state wherein the torsion angles of the carbons directly bound to the heterocyclic nitrogen would position the rest of the side chain, allowing for the formation of distinctly oriented, interdigitated *n*-alkyl chains.

The single-crystal structures of 1-dodecyl-3-methylimidazolium bromide[30] ($[C_{12}C_1im][Br]$) and 1-dodecyl-3-methylimidazolium chloride ($[C_{12}C_1im][Cl]$)[31] have both been reported. While the dodecyl structure had shorter alkyl chains than those reported by Hardacre (*vide supra*), a number of similar features were observed, including the formation of layers *via n*-alkyl chain interactions and the observation of varied torsion angles in the side chains. Additional crystal structures of structurally related halide-based ILs have since been reported, all sharing similar short and long-range features.[32–34] However, of particular note is that the CSD currently does not have any imidazolium-based IL structures with long saturated alkyl chains that are anhydrous.[35,36] Further, while most of the reported structures are of the $[C_n mim]$ cations when $n \geq 10$, few reports currently exist using the dmim heterocycle as a cation with halide counter ions despite the favorable properties the dmim cation can impart.[37] Recently, the Mudring group has reported the synthesis and characterization of several asymmetrical dmim-based ILs with long alkyl chains.[38] These dmim-based ILs displayed higher melting and clearing points while displaying increased hydrophobicity when contrasted with ILs based on methylimidazolium headgroups.

By definition, the crystalline state of ionic liquids is well-ordered and provides an opportunity to study the intermolecular interactions between cations and anions in detail. It is understood that upon melting, specific intermolecular interactions (*i.e.*, hydrogen bonding, π-stacking, *etc.*) are still present in addition to the dominant coulombic attractions.[23] However, questions remain about the structure and interactions within the solution and liquid structure of IL. As discussed, the structure and physicochemical properties of alkyl-chain bearing ILs has been studied quite extensively to date. Comparatively few studies, though, have experimentally assessed the non-covalent interactions derived from the crystal structures and correlated these findings with the solution phase for this class of compounds. There have been reports wherein the solution and solid-state structure of ILs have been studied. For example, an early report by the Hardacre group examined the structure of short-chain ILs in aromatic solvents.[39] Their studies found that the benzene solvent displaced the anions and increased the distance between the cations in solution.

Using molecular dynamics simulations, Wang and Voth proposed that long-chain ILs would form aggregates driven by intermolecular interactions.[40] Work by Balevicius *et al.* demonstrated, *via* NMR spectroscopy, that solutions of $C_{10}C_1im][Br]$ formed hydrogen bonding networks between the cations and anions in methanol and water solutions.[41] By incorporating calculated models of their ILs, the Balevicius group was able to conclude that within solution ordering of the cations is retained, to a degree. These studies demonstrate that due to the complexity of the solution and liquid phases of ILs, knowledge drawn from crystallographic interactions can play a key role in interpreting and understanding experimental data of the solution state for ILs, leading to a more thorough understanding of these functional materials.

The importance of understanding aggregation in ILs cannot be overstated in materials science. It influences the electronic and optical properties, as well as the processability of bulk materials. With the goal of investigating how the thermal and crystal packing behavior correlates with aggregation in the solution phase, the current work uses ultraviolet-visible (UV-vis) spectroscopy as a facile tool for probing self-assembly in organic solutions. This approach was extensively used by Würthner in the field of small-molecule electronics to draw similar correlations between solid and solution phase aggregation in cyanine dyes.[42] In these studies, aggregation was probed with

optical methods. It was observed that highly polarizable dyes could generally self-assemble in various configurations that can enhance or attenuate dipolar interactions in the solid phase. These aggregates often produce diagnostic changes in the UV-vis absorption spectrum, as either bathochromic or hypsochromic shifts in the λ_{max} or the loss of the fine structure of vibronic transitions with concentration or solvent polarity changes. These changes in the absorption spectra thus can be correlated with the formation of aggregates in solution.

Herein we report the synthesis, thermal analysis, structural characterization, and solution studies of four [$C_{16}C_1C_1$im]-based ILs (figure 1). Two of the crystal structures are of the halide salts (Br^-, and I^-), and the third structure uses the bis(trifluoromethane)sulfonimide (Tf_2N^-) anion,[43] one of the most commonly utilized anions in the field of ILs. We investigated the single-crystal structures of the bromide, iodide, and Tf_2N^- derivatives to evaluate the interactions and long-range ordering of the compounds in the solid-state, providing vital data useful for the development of predictive models.[22,44] Hirshfeld surface analysis[45] of the three crystal structures is also provided, allowing for a more detailed analysis of how systematic changes in the anion impart the interactions present in the assemblies. The crystallographic and surface data are supplemented with thermal data (thermogravimetric analysis and differential scanning calorimetry), providing a thorough evaluation of the structure and properties of these new compounds. The solid-state structures of the compounds are correlated to the solution structures *via* UV-vis spectroscopic studies. The combination of solid-state and solution studies allows for a thorough investigation into the unique properties imparted by the changes in the anions in the compounds.

2. Materials and Methods

2.1 Chemicals

1,2-Dimethylimidazole, 1-chlorohexadecane, 1-bromohexadecane, and 1-iodohexadecane were purchased from Fisher Scientific. Lithium bis(trifluoromethane)sulfonimide was purchased from TCI. Solvents were purchased from Acros Organics and Oakwood Chemical and used as is without further purification.

2.2 Spectroscopy

^{1}H, ^{13}C and ^{19}F NMR spectroscopy was performed on a JEOL 400 MHz NMR. NMR solvents were purchased from Cambridge isotope labs. NMR shifts are referenced to residual undeuterated solvent peaks. Solution-phase UV-vis spectroscopy studies were performed in HPLC grade acetonitrile, chloroform (stabilized with ethanol), and methanol solvents.

2.3 Thermal Properties

Melting points, glass transitions, and crystallization temperatures were measured using a TA instruments Q200 differential scanning calorimeter (DSC). Each sample was placed in an aluminum pan and cycled three consecutive times from -50 °C to 150 °C at a heating and cooling rate of 10 °C/min. A three-minute isothermal step was included at the minimum and maximum temperatures of each cycle.

For compound **3**, a Mel-Temp melting point apparatus was used to visually track any changes during a heating cycle. A quartz capillary tube was loaded with a small amount of **3**, packed, and then placed into the instrument. The instrument was set to 4 (dial values 1 – 10) and allowed to heat with the sample inside.

Decomposition temperatures were measured on a TA instruments Q500 thermogravimetric analyzer (TGA) using the default dynamic settings for the system and using a platinum pan. The differential thermogravimetric curves (DTG) were obtained from the experimental TGA data and visualized with the OriginPro software. Decomposition temperatures ($T_{decomp.}$) were obtained using the maximum thermal decomposition rate of each DTG curve.

2.4 Single Crystal Diffraction

Single crystals of compounds were coated with Fomblin oil and transferred to the goniometer of a Bruker D8 Quest diffractometer with a Cu Kα wavelength (λ = 1.54178 Å) I-μ-S microsource X-ray tube, laterally graded multilayer (Goebel) mirror for monochromatization, and a Photon III C14 area detector. Examination and data collection were performed at 150 K. Data were collected, reflections were indexed and processed, and the files scaled and corrected for absorption using APEX3[46], SAINT and SADABS.[47]

For all compounds the space groups were assigned using XPREP within the SHELXTL suite of programs[48,49] and the structures were solved by dual methods using SHELXS[48,49] or SHELXT[50] and refined by full matrix least squares against F^2 with all reflections using Shelxl2018[51] using the graphical interfaces Olex2[52] and/or ShelXle.[53] Carbon bound H atoms were positioned geometrically and constrained to ride on their parent atoms. C-H bond distances were constrained to 0.95 Å for aromatic and alkene C-H moieties, and to 0.99 and 0.98 Å for aliphatic CH_2 and CH_3 moieties, respectively. Methyl H atoms were allowed to rotate, but not to tip, to best fit the experimental electron density. U_{iso}(H) values were set to a multiple of U_{eq}(C) with 1.5 for CH_3, and 1.2 for C-H and CH_2.

Crystals of **3** consisted of extremely thin plates. All crystals were multiply twinned. Crystals closest to single were found to be twinned by a combination of non-merohedral and pseudo-merohedral twinning. Non-merohedral twinning was identified using the program Cell_Now, with the two components being related by a 180° rotation around the reciprocal (1 0 0) axis and confirmed later by the program Rotax[54] as implemented in WinGX[55] (transformation matrix 1 0 0.188, 0 -1 0, 0 0 -1).

Poor diffraction peak shape with very elongated and smeared out peaks, especially at high angle, made simultaneous integration of both twin domains using SAINT problematic due to excessive multiple overlap of reflections, resulting in large numbers of rejected reflections. Attempts were made to adjust integration parameters to avoid excessive rejections (through adjustments to integration queue size, blending of profiles, integration box slicing and twin overlap parameters), which led to less but still substantial numbers of rejected reflections. With no complete data set obtainable through simultaneous integration of both twin domains, the data were instead handled as if not twinned, with only the major domain integrated, and converted into an hklf 5 type format hkl file after integration using the "Make HKLF5 File" routine as implemented in WinGX. The twin law matrix was used as obtained from SAINT, see above. The Overlap R1 and R2 values used were 0.37, i.e. reflections with a discriminator function less or equal to overlap radius of 0.37 were counted as overlapped, all others as single. The discriminator function used was the "delta function on index non-integrality". No reflections were omitted.

Additional twinning by pseudomerohedry was identified using Rotax in WinGX to be by a 180° rotation around the direct (1 0 0) axis (transformation matrix 1 0 0, 0 -1 0, 0 0 -1). The twinning was applied using the program 2Twin[56] to create an HKLF 5 type file with four twin components.

The structure was solved using direct methods (SHELXS) from the original hklf4 data. Initial refinement against these data gave R values around 22% for R1. Refinement against data corrected only for twinning by pseudomerohedry gave R values around 14%, refinement against data corrected only for twinning by non-merohedry gave R values around 12%.

The structure was refined using the hklf 5 routine with all reflections of component 1 (including all overlapping reflections), resulting in a BASF values of 0.266(6), 0.086(4) and -0.015(7), indicating absence of the forth twin domain (with simultaneous presence of both non- and pseudo-merohedral twinning).

No R_{int} value is obtainable for the hklf 5 type file using the WinGX routine. The value from refinement against uncorrected data is given instead.

For compound **4**, both anions and cations are disordered over each two moieties. For the cations, all four moieties were restrained to have similar geometries. For the anions, major and minor moieties were each restrained to have similar geometries. U_{ij} components of ADPs for disordered atoms closer to each other than 2.0 Å were restrained to be similar. Subject to these conditions the occupancy ratios refined to 0.545(4) to 0.455(4) for cation A, to 0.562(4) to 0.438(4) for cation B, to 0.856(4) to 0.1444) for anion A and to 0.868(4) to 0.132(4) for anion B.

Complete crystallographic data, in CIF format, have been deposited with the Cambridge Crystallographic Data Centre. CCDC 2218608-2218610 contains the supplementary crystallographic data for this paper. These data can be obtained free of charge from The Cambridge Crystallographic Data Centre via www.ccdc.cam.ac.uk/data_request/cif.

2.5 Software

Hirshfeld surfaces, images, and fingerprint plots were calculated and produced using CrystalExplorer21.[57] Images and analysis of the structures was accomplished using Olex2 and Mercury.[58] The supplemental information contains the fingerprints and images of the surfaces calculated from the Hirshfeld analysis. Note that for π interactions, C and N atoms are discussed as points of interaction as these are the atoms present in the heterocyclic imidazolium ring.

Void space analysis was completed using Mercury with a 0.7 Å probe radius and a 0.2 Å grid spacing. Voids were calculated using the contact surface option. The void space analysis of **4** was omitted due to the disorder in the crystal.

For all images shown of the crystal structures the following color scheme is used to represent atoms: carbon = gray; nitrogen = blue; hydrogen = white; fluorine = green; oxygen = red; bromine = tan; iodine = purple.

2.6 Synthesis

*1,2-Dimethyl-3-hexadecylimidazolium chloride (**1**)*
0.200 grams (2.1 mmol, 1 equiv.) of 1,2-dimethylimidazole and 0.753 mL (2.5 mmol, 1.2 eq.) 1-chlorohexadecane were added to a glass vial containing a stir bar. The flask was sealed and heated at 90 °C overnight with stirring. After this, the reaction was allowed to cool to room temperature during which the reaction solidified into a white solid. The white solid was filtered and washed with ethyl acetate (3 × 25 mL), hexane (3 × 25 mL), and diethyl ether (3 × 25 mL). The product was heated (50 °C) under vacuum to remove any solvents, yielding a fine, white powder (0.355 g, 47 %). No single crystals suitable for X-ray structural analysis could be found, though the compound did crystallize from methyl ethyl ketone.
^{1}H NMR (400 MHz; $CDCl_3$) δ 7.74 (s, 1H), 7.42 (s, 1H), 4.14 (t, J = 7.4 Hz, 2H), 3.97 (s, 3H), 2.73 (s, 3H), 1.76—1.73 (m, 2H), 1.27—1.20 (m, 26H), 0.83 (t, J = 6.4 Hz, 3H).^{13}C NMR (101 MHz; CD_3OD): δ 145.8, 123.6, 122.2, 35.4, 33.1, 30.9, 30.8, 30.8, 30.7, 30.7, 30.6, 30.5, 30.2, 27.4, 23.8, 14.4, 9.5

*1,2-Dimethyl-3-hexadecylimidazolium bromide (**2**)*
Compound **2** was synthesized using the same procedure as for **1**, but with 1-bromohexadecane as the alkylating agent. White solid (0.692g, 82%).Single crystals suitable for X-ray diffraction were grown from slow diffusion of diethyl ether into a saturated solution of the compound dissolved in isopropyl alcohol.
^{1}H NMR (400 MHz; CD_3OD) δ 7.53 (d, J = 2.0 Hz, 1H), 7.48 (d, J = 1.9 Hz, 1H), 4.15 (t, J = 7.4 Hz, 2H), 3.83 (s, 3H), 2.63 (s, 3H), 1.83 (q, J = 7.0 Hz, 2H), 1.37—1.29 (m, 26H), 0.90 (t, J = 6.7 Hz, 3H).
^{13}C NMR (101 MHz; CD_3OD): δ 145.8, 123.6, 122.2, 35.5, 33.1, 30.8, 30.8, 30.8, 30.8, 30.7, 30.6, 30.5, 30.2, 27.4, 23.8, 14.5, 9.6.

*1,2-Dimethyl-3-hexadecylimidazolium iodide (**3**)*
Compound **3** was synthesized using the same procedure as for **1**, but with 1-iodohexadecane as the alkylating agent. White solid (0.741g, 79%).Single crystals suitable for X-ray diffraction were grown from slow diffusion of methyl tert-butyl ether into a saturated solution of the compound dissolved in ethanol.

^{1}H NMR (400 MHz; CD_3OD) δ 7.54 (d, J = 2.1 Hz, 1H), 7.48 (d, J = 2.1 Hz, 1H), 4.16 (t, J = 7.5 Hz, 2H), 3.83 (s, 3H), 2.65 (s, 3H), 1.85—1.82 (m, 2H), 1.29 (s, 26H), 0.90 (t, J = 6.8 Hz, 3H).
^{13}C NMR (101 MHz; CD_3OD): δ 145.8, 123.6, 122.2, 35.6, 33.1, 30.9, 30.8, 30.7, 30.7, 30.6, 30.5, 30.4, 30.2, 27.4, 23.7, 14.5, 9.9.

*1,2-Dimethyl-3-hexadecylimidazolium bis(trifluoromethane)sulfonimide (**4**)*
A 0.20 gram sample of **2** was added to 30 mL of water in a glass vial containing a stir bar. To this solution was added 0.17 grams of lithium bis(trifluoromethane)sulfonimide. The vial was sealed and stirred at 50 °C overnight. The reaction was cooled to room temperature and the white solid filtered and washed with water (5 × 25 mL). The solid was collected and dried under vacuum to remove any residual water (0.15 g, 76%).Single crystals suitable for X-ray diffraction were grown from slow evaporation of a solution of the compound dissolved in isopropyl alcohol.

^{1}H NMR (400 MHz; $CDCl_3$) δ 7.20 (d, J = 1.9 Hz, 1H), 7.15 (d, J = 1.9 Hz, 1H), 4.02 (t, J = 7.6 Hz, 2H), 3.79 (s, 3H), 2.59 (s, 3H), 1.77 (t, J = 6.8 Hz, 2H), 1.26 (d, J = 27.5 Hz, 26H), 0.87 (t, J = 6.7 Hz, 3H).^{13}C NMR (101 MHz; $CDCl_3$) δ 143.8, 122.7, 120.9, 124.7—115.1, 48.9, 35.4, 32.0, 29.8, 29.8, 29.7, 29.7, 29.6, 29.48, 29.5, 29.1, 26.4, 22.8, 14.2, 9.7
^{19}F NMR (376 MHz; $CDCl_3$): δ −78.89 (s).

3 Results and Discussion

3.1 Single Crystal Structural Analysis

Single crystals suitable for diffraction were grown for compounds **2**, **3**, and **4**. Compounds **2** and **4** crystallize in the $P\bar{1}$ space group and **3** in the $P2_1/c$ space group. Both **2** and **3** have a single ion pair in the asymmetric unit, while **4** has two disordered ion pairs (labeled A – D in Figure S1) in the asymmetric unit. For analysis and discussion regarding compound **4**, both interacting sets of molecules, that is A&C and B&D, were used for analysis. Neither structures **2** nor **3** have any disorder in the asymmetric unit.

Compound **2** has a rod-like shape which is broadly defined by the orientation of the alkyl chain with respect to the cationic core (Figure 2).[59] The alkyl-imidazolium core plane angle is 92.93(10)°. The alkyl chains in **2** are oriented to form parallel end-to-end arrangements with little observed interdigitation (Figure 3). Concerning cation-anion interactions, both of the aromatic hydrogens, that is C4—H and C5—H, are seen interacting with the bromide ion at approximately the same distance of 2.73 Å (d(H···Br)). The bromide ion, in turn, forms interactions with six surrounding cationic imidazolium rings through a series of interactions with both methyl groups on the ring. The distances for the H···Br interactions with the methyl hydrogens range from 2.72 Å to 3.42 Å, meaning that the bromide ion is capable of interacting with both aryl and alkyl hydrogens of the imidazolium core. In addition to the H···Br and H···H interactions from the alkyl chain, π···π interactions (d(π···π) = 3.59 Å; centroid···centroid) help form the long range ordering of the molecules in the crystalline state.

Compound **3** (Figure 4) has a planar-like arrangement wherein the alkyl group is oriented in approximately the same plane as the imidazolium ring, with a core-plane angle of 153.2(9)°. Effectively, the alkyl chain is oriented

in the same direction as the methyl group attached to the C2 position of the imidazolium core. The alkyl chain of compound **3** has a 'crank-handle' conformation on the carbon atoms closest to the imidazolium ring. The term 'crank-handle' was used by De Roche *et al.* to describe the unique conformation of the chain due to the dihedral angles in the carbons near the imidazolium ring of long-chained ILs.[60] This name simply refers to the arrangement of the carbon atoms wherein a gauche orientation is observed in carbons C6 – C9. The remaining carbons in the hexadecyl chain, that is C10 – C21, are all in the expected staggered conformation. This twisting in the alkyl chain is likely due to steric interactions arising from the drive to maximize the inter-alkyl H···H interactions by allowing for interdigitation (see Figure 5). The alternating interdigitated arrangement of the alkyl groups also allows for interactions between the terminal methyl group on the alkyl chain (C21—H) and the methyl groups on the cation (C5—H). These methyl H···H interactions range from 2.65 Å to 2.91 Å (*d*(H···H)).

Similar to **2**, the iodide anion is surrounded by six cationic moieties, effectively placing the anion in a positively charged pocket within the crystal. The iodide anion forms the expected interactions with the aryl hydrogens C4—H and C5—H at distances ranging from 2.96 Å to 3.59 Å (*d*(H···I)). The alkyl interactions arising from the crank-handle conformation of the carbon atoms causes the imidazole rings to orient in a manner wherein no observed π···π stacking is seen. However, there are longer H···π interactions observed from the C7—H methyl group on a symmetry adjacent imidazole (*d*(H···π) = 3.25 Å).

Compound **4** is the most complex of the structures due to the four ion pairs in the asymmetric unit (Figure 6). Overall, **4** shares structural features observed in both **2** and **3**. For example, the alkyl chains in **4** form interdigitated layers similar to those observed in **3** (see Figure 7). Additionally, the orientation of the alkyl chains in **4** gives an overall linear structure wherein the alkyl chain is oriented in approximately the same plane as the imidazolium core, comparable to what was observed in **3**. Similar to compound **2**, cations A, B, and C show only a staggered conformation of the alkyl chain. Cation D; however, has a unique gauche arrangement of the alkyl chain in the 'symmetry-breaking' region of the chain.[61] Despite the similarities in arrangement, a closer look at the carbons of the alkyl chain is helpful for distinguishing the varied orientations of the alkyl chain.

Table 1 lists a series of torsion angles to help establish the unique arrangements of the C_{16} chains in the asymmetric units for all the compounds. For the structures presented herein, these carbons (C8 – C11) show several distinctive arrangements as described previously. For example, in compound **2**, the entire alkyl chain exists in a staggered arrangement, with no deviations from the expected torsion angles (~180°) in sp^3 methylene groups. However, **3** shows a torsion angle of 60.0(3)° at the C8—C9—C10—C11 position. The gauche conformation at this position in the alkyl chain causes a significant change in the overall arrangement of the alkyl chain with respect to the heterocycle. The torsion angles at the C8 through C11 position set the orientation of the alkyl chain, allowing for distinctive arrangements for the ILs. However, the remaining carbons in the chains after C11are all in the staggered conformation. These conformational trends also remain true for all three of the structures examined. The 'crank-handle' region of the alkyl chain, thus, is the only area in which differing arrangements of carbon atoms are observed in the solid state. This observation is in line with previously reported structures,[34,62,63] wherein the majority of the alkyl chain exists in the staggered conformation and the carbons closest to the heterocycle is where deviations tend to occur. López-Martin *et al.* elaborate on the different portions of the alkyl chains in ILs.[61] Specifically, they mention the region nearest to the imidazolium core as the area allowing for asymmetry in the structure. Breaking of symmetry *via* the alkyl chain carbons near the imidazolium ring lowers the melting points of the ILs.

To summarize, several key structural features are observed when examining the molecular and crystal structures of these compounds. First, the *n*-alkyl chain H···H interactions are the dominant force leading to the arrangement of the molecules. However, it should be stated that the coulombic interactions are likely far stronger in their contribution to the lattice stabilization energy, even with the larger alkyl chains.[64] Second, the alkyl chains show diverse arrangements with respect to the torsion angles in the symmetry breaking region of the chain. Third, the anions are observed to interact with all sets of hydrogens in the structure including both aromatic and aliphatic hydrogens. Finally, differing types of π interactions are observed in all three of the structures consisting of a combination of H···π, anion···π, and π···π stacking, to varying degrees.

3.2 Hirshfeld Surface Analysis

To better visualize the distinct interactions and arrangements of the cations, we performed Hirshfeld surface analysis on the three crystal structures, and the fingerprints from the surface analysis are shown in Figure 8. Examining the complete fingerprints helps clarify the unique arrangements of the cations while also highlighting the general similarities between the structures. For example, all of the cations are dominated by the alkyl H···H interactions which are readily visible as the bright green and red regions of the fingerprint plots. In brief, the fingerprints' colors correspond to the number of interactions falling into those distances (d_i and d_e).[65] The alkyl interaction account for nearly 90% of the total interactions observed in compounds **2** and **3**. Thus, it follows that the slightly higher energetic gauche conformer observed in **3** is preferred so as to maximize the favorable H···H interactions. For compound **4**, the H···H interaction percentage is significantly lower (~67%). This lower percentage is a direct result of the inclusion of the larger Tf_2N^- anion in **4** as compared to the monoatomic anions in **2** and **3**. Further, this observation helps explain, in part, the lower melting point for compound **4** (*vide infra*).

Aside from the alkyl H interactions, information about the long-range ordering of the cations is also available when examining the fingerprints on a per-atom basis. For example, π interactions have long been known as stabilizing interactions in crystals of organic molecules and in ILs.[66–68] Examining the H···C|C···H, N···C|C···N and C···C interaction fingerprints for compounds **2** – **4** reveals the unique π interaction motifs in each compound. Figure 8 shows these fingerprints for all of the compounds.

Compound **3** displays nearly double the percentage of H···C|C···H π interactions when compared to **2** (2.1% for **2** and 4.2% for **3**). In both cases, that is with **2** and **3**, these H···C|C···H interactions arise from the methyl hydrogens interacting with the imidazolium heterocycle. The arrangement of the cations with respect to other cations is what leads to these differing interactions. Examining the packing diagrams for **2** and **3** (figures 3 and 5 respectively) offers a visualization of these arrangements and figure S2 and S3 offer zoomed-in view of the H···C|C···H interactions for both **2** and **3**. The interaction distances in **2** range from approximately 3.045 - 3.429 Å while in **3** they range from 2.884 - 3.070 Å. Not only are the distances shorter for **3** but the geometry of the interactions is distinct from **2**. Essentially, the H···C|C···H interactions in **2** arise from close contacts due to the head-on stacking arrangement of the cationic heterocycles. In **3**, however, the methyl groups on the imidazolium ring are interacting with the π system of the ring with no stacking observed, leading to the different geometries of these interactions.

To further examine the π interactions the N···C|C···N and C···C fingerprints are shown in figure 8. The fingerprints for **2** show a distinct set of regions of interactions indicative of π-π interactions arising from off-center parallel cation-cation interactions.[67] The slight percentage of C···C interactions in **3** arise from residual contacts of the cations.

Notably, compound **4** does not exhibit any H···π interactions. Instead, compound **4** displays F···π and O···π interactions from the Tf_2N^- anion. The disorder in the asymmetric unit does make examining and discussing exact interactions challenging. However, both sets of cations, that is **4A** & **4C** and **4B** & **4D**, display overall comparable O···π and F···π interactions ranging in distances of 3.19 – 3.50 Å. Figure 9 shows a depiction of these interactions with one set of the disordered cations and anions as a representative depiction for the structures. In contrast, **2** and **3** show little anion···π interactions. This is reflected in the negligible percentages of interactions observed in the fingerprints in Figure 10.

In summary, two key interactions and distinctions are drawn out through Hirshfeld surface analysis. First, is that the alkyl chains are shown to adopt less energetically favored conformations to maximize H···H interactions of the alkyl chains. Second, the halide anions do not show any significant anion···π interactions, whereas the Tf_2N^- anions are seen interacting via both sulfonyl oxygen and fluorine moieties. It should be noted that previous reports have observed halide···π interactions in ILs.[69,70]

3.3 Crystalline Void Space

Given the unique geometries and lack of disorder in **2** and **3**, the void space of the two structures was compared to help draw out any noteworthy distinctions. The void space in ILs has been shown to influence physical properties.[71] Further, examining the free volume of ILs is a useful metric for evaluating the structure and properties of these materials,[72] thus analysis of the crystalline volume is a useful point of comparison. The void space for **2** and **3** is 93.57 $Å^3$ (8.3 % of unit cell) and 151.44 $Å^3$ (6.6 % of unit cell), respectively (figures 11 and 12). One similarity in the overall positioning of the void space is that in both structures, a significant portion of the void space surrounds the anion. Further, there is little void space around the majority of the alkyl chains, pointing towards the efficient packing of the alkyl chains. This observation complements the surface analysis which shows that the H···H interactions are a significant driving force for crystal packing.

A more subtle difference in the location appears from the arrangement of the alkyl chains in **2** *vs* **3**. As discussed, the alkyl chain in **2** is linear, while in **3** a gauche arrangement of atoms is observed (*vide supra*). Close examination of the voids surrounding the cation reveals a set of voids appearing due to the unique conformation in **3**. The changes in the alkyl chain geometries introduces some inefficient packing with respect to the anion-cation interactions yet allows the alkyl chains to pack more efficiently. Further, it has been shown in previous studies that free space in solids and liquids allows for free motion of molecules.[73–75] The increased void space in **3** could account for the complex thermal behavior observed, given the more accessible motion of the molecules and anions (*vide infra*).[76] Particularly within this set of molecules, it is observed that the imidazolium heterocycle can rotate, vis-à-vis the observed disorder in **4**, allowing of distinct orientations of the cationic head.

3.4 Thermal Analysis

The TGA and derivative curves (dTG) are shown in Figure 13. The decomposition temperatures for the compounds adhere to the expected trends, following previously reported data for related ILs.[77] The halide ILs **1** – **3** show the expected increase in decomposition temperature following the periodic trend, with the **1** having the lowest $T_{decomp.}$ (257 ºC), followed by **2** (267 ºC) and **3** (282 ºC). Expectedly, the Tf_2N^- based compound (**4**) has a significantly higher $T_{decomp.}$ at 419 ºC, a well-documented observation from the IL literature.[78] A few key details can be inferred from the decomposition profiles. First, the decomposition pathway appears to be the same for compounds **1** – **3**, given that the identical curves show only a single, complete decomposition step. Second, the

decomposition of **4** shows two unique peaks, with the maximum for each peak being 419 ºC and 427 ºC, respectively. This two-step decomposition could be a result of the Tf_2N^- anion decomposition as well as cation decomposition.[79] Contrasting these decomposition profiles for the different compounds points to a unique pathway for the halides *vs.* the Tf_2N^- based anion compounds.[80]

The DSC traces for compounds **1**, **2**, and **4** are shown in figure 14. Compounds **1**, **2**, and **4** show a distinct melting transition in all three of the heating cycles. Compounds **1** and **2** have nearly identical melting points at 101 °C and 100 °C respectively. As expected, the melting point for **4** is significantly lower given the inclusion of the Tf_2N^- anion *vs.* the halides (T_m = 66 ºC). All of these compounds then show distinct crystallization temperatures on the cooling cycles also, though the crystallization temperature does shift for compound **4** for the first cycle *vs.* the other two cycles (see supplemental information). This shift is not unusual, however, given the presence of thermal history and the often complex crystallization kinetics of ILs in general.[81,82]

Compound **3** displays the most complex set of phase transitions of the compounds discussed herein. The individual heating and cooling traces are shown in Figure 15. Multiple exothermic transitions occur, ranging from approximately 65 °C to 120 °C for all three heating cycles. Visual inspection of a heating cycle shows that the lower temperature transitions at 71 °C, 78 °C, and 98 °C show no observable changes in the material. Likely, these transitions correspond to mesophases related to changes in orientations of the alkyl chains and/or associations with the iodide anion.[38,82] Given the multiple orientations of the alkyl chains shown in the crystal structures presented herein, this observation could point to the likely existence of multiple crystalline or solid-state phases of compound **3**. As previously reported for structurally related ILs, low-temperature smectic phases and multiple crystalline states exist.[83] A more rigorous study of these transitions using appropriate techniques would be required (e.g., polarized microscopy).[84]

3.5 Solution Studies

In order to investigate the solution-phase ordering of **1**-**4**, UV-vis spectroscopy was used to probe any assembly changes in organic solvents. Compounds were dissolved in acetonitrile and diluted to 50 µM. The resulting absorption spectra in Figure 16a demonstrate significant changes in the profile and molar absorptivity. Compounds **1** and **4** show no absorption bands in the UV-vis spectral region, whereas compounds **2** and **3** show differently structured absorption bands between 250 and 300 nm. Additionally, both of these compounds show a lower energy absorption band above 400 nm, which has been attributed to micelle formation in surface-active ionic liquids.(SAILs, see ref 86) This result is consistent with a change in assembly for the series of compounds as the ionic radius of the counter-anion changes.

In order to probe the self-assembly behavior further, the solutions of **1** – **4** were concentrated two-fold in acetonitrile to 100 µM (as shown in Figure 16b-e). For **1** and **4**, there was no significant change in the absorption profile. For **2**, the absorption at 210 nm is present, in addition to a higher energy band at 201 nm. For **4**, the same bands are present at 210 and 201 nm; however, an additional low-energy band at 247 nm increases in size with increased concentration. Previous studies have shown these bands can be attributed to electronic transitions involving the π system of the imidazolium cation. These results correlate with the anion affinity for the polar head group, wherein Tf_2N^- and Cl anions generally have a stronger affinity and result in tighter ion pairing in nonpolar solvents. The bromide and iodide anions have larger atomic radii and are more diffuse, so they tend to associate more with the alkyl chain.[85] This result is consistent with previously reported work characterizing the critical micelle concentrations of SAILs in protic solvents[86], and this observation also is consistent with the discussion

of π interactions in the crystalline state (*vide supra*), thus suggesting that the absorption bands at 201-210 nm of **2** and **3** originate from ion pairs being more diffuse than in **1** and **4** in hydrophobic solvents. The Beer-Lambert plots for compounds **2** and **3** at λ_{max} of 209 nm show little to no change in slope with increased concentration; however, a new series of absorption bands appear above 400 nm for **2** and **3**, whose absorbance does not obey the Beer-Lambert relationship.

In order to further investigate the different modes of assembly for anions with different atomic radii, solvent studies were performed on the halide series **1** – **3** by adding a protic solvent (methanol) to a chloroform solution of the IL. Chloroform is a relatively nonpolar solvent when compared with acetonitrile, so it was expected that the addition of a polar protic solvent such as methanol would alter the interactions between the ILs in solution.[87] As shown in Figure 17a, compound **1** shows no changes in the absorption spectrum with addition of methanol. Methanol should be able to solvate hard ions, with chloride being solvated more strongly in protic solvents than the more diffuse anions bromide and iodide. In a solvent with a low dielectric constant like chloroform, there is no absorption observed between 200-210 nm for any of the halide counterion series. Instead, only the absorption at 247 nm is observed for both **2** and **3**, with additional low-energy bands appearing around 300 nm for **3** (as shown in Figures 17b and c). When methanol is added, the absorption band at 247 nm decreases. This result suggests that the smaller anions with tighter ion pairing in chloroform do not produce the absorption that is observed in acetonitrile which has a higher dielectric constant than chloroform. Furthermore, the existence of additional low energy absorption bands for **3** in chloroform solvent suggests a new type of assembly. Upon addition of higher concentrations of methanol, these bands decrease. This phenomenon is consistent with previously reported critical micelle concentration solvent studies for SAILs with varied counter-anions.[86] In our present solvent studies, it is noted that the appearance of new low-energy bands in the absorption spectra above 300 nm is consistent with micelle formation.

To summarize, the solution studies of these compounds corroborate several observations from the crystalline solid-state. First, anion size was found to lead to different assemblies of the compounds in solution. To the point, different geometries, alkyl orientations, and anion interactions were observed in the solid-state leading to distinct structures. Second, anion$\cdots\pi$ interactions from Tf_2N^- were found to be observable experimentally. Furthermore, the lack of absorption bands in the UV/vis spectra for **1** and **4** could point to $Cl^-\cdots\pi$ interactions existing in the crystalline state, though more rigorous studies will be needed to verify this conclusion. Finally, distinct assemblies of **3** were observed in solution when compared with **1** and **2**. This may shed light on the thermal behavior of **3** wherein multiple phase transitions are observed.

4 Conclusions

A study of lipid-like 1,2-dimethylimidazolium ionic liquids was accomplished using a combination of crystallographic and solution studies. The solid state structures were examined using Hirshfeld surface analysis to draw out distinct interactions leading to the formation of the crystals. Further, the thermal data of the compounds were collected, allowing for a thorough understanding of the fundamental properties and interactions within these new compounds. Through careful examination of the data, several key conclusions are drawn from the experiments.

- All three of the crystal structures examined herein display a unique arrangement of the alkyl chain, specifically with respect to the conformations of the carbon atoms near the imidazolium ring. The alkyl-core plane angles lead to a rod-like structure for **2** and a pseudo-planar structure for **3** and **4**. Compounds **2** and **4** show completely

staggered alkyl chains, while **3** shows a gauche conformation in the symmetry-breaking region of the chain. Given the general similarities of the these compounds, it is likely that multiple conformations of the alkyl chain can exist for any of the structures examined pointing towards the probability of conformational polymorphs existing. Further, these alkyl conformations also give a view of the possible arrangements of the alkyl chains in solutions.

- Hirshfeld surface analysis of the compounds revealed that alkyl chain packing is a controlling force in crystal structure formation. For each compound examined, approximately 90% of the total non-covalent interactions arose from H···H interactions predominantly from the alkyl chains for the halide-containing compounds. This value decreased, however, for **4,** wherein approximately 60% of the interactions arose from the alkyl chains. Concomitantly, the melting point of **4** is lower than those of the halide compounds though this decrease in melting point is not exclusively due to H···H interactions.
- Several distinct π interaction motifs are observed. The halide-based structures show multiple cation-cation interactions, both π-π stacking and CH_3···π interactions. Compound **4**, on the other hand, shows none of these interactions but instead has O···π and F···π interactions from the anion.
- The thermal behavior of the compounds is, for the most part, predictable and follows established trends for ILs. For example, the halide-based compounds (**1** – **3**) have lower decomposition temperatures than the perfluoroalkyl-containing structure **4**. This predictability also holds true for the compounds with well-defined melting transitions wherein the halide compounds have higher temperature phase transitions than the Tf_2N^- compound. Most notably, compound **3** is an outlier, displaying five detectable phase transitions in the heating phase of the DSC cycles. Visual inspection of a heating cycle yielded no conclusive results aside from an observable melting point. Thus a more detailed study will need to be completed to determine the nature of these transitions.
- Solution studies were completed to help further understand the structural properties of these compounds. Overall the solution phases of these compounds correlate with the crystalline state. Anion···π interactions were observed in solution and followed the observations in the crystals. The solution studies suggest that the chloride-bearing compound (**1**) would display anion···π interactions. Additionally, multiple assemblies of **3** were found in solution, offering additional insight into the DSC data. Unfortunately, no suitable single crystals of this compound were obtainable to verify this observation. Moreover, the concentration of the *cmc* in protic solvents appears to the largest for hydrophilic anions like chloride ion, and the *cmc* is lowest for hydrophobic anions like iodide ion.

The work presented herein provides a strong foundation for future studies with this class of compounds. As stated, there are several key structural points which remain in question. For example, successful growth of a single crystal of **1** would help verify our hypothesis about the existence of π interactions with the anion in the solid-state. Further, a more rigorous thermal analysis of **3** would help shed light onto the relationship between free volume in the crystal and if the multiple phase transitions are related to alkyl chain rearrangements as postulated. Finally, we are further investigating the solution of 1 – 3 to clearly identify the self-assembly properties in solution.

Acknowledgements

S.B. and P.C.H. would like to thank Michael and Lisa Schwartz for their generous financial support of the undergraduate research program in the department of Chemistry and Physics at AMU. S.B. and P.C.H. would also like to thank Joe and Karen Townshend for their generous financial donation used in the purchase of research instrumentation in the department of Chemistry and Physics at AMU. A.M. is grateful to the Richard S. Shineman Foundation and the Oswego College Foundation for the generous financial support. P.C.H. wishes to thank Florida Gulf Coast University for the use of their instrumentation.

Funding

Acknowledgment is made to the Donors of the American Chemical Society Petroleum Research Fund (66195-UNI10) for support of this research. This work is partially supported by the National Science Foundation under Grant No. CHE–1530959 (MRI) and CHE–1952846 (RUI). This work was supported by Ave Maria University Department of Chemistry and Physics.

CRediT Statement

Sophia A. Bellia: Methodology, Formal Analysis, Resources, Investigation
Matthias Zeller: Methodology, Validation, Formal Analysis, Investigation, Resources, Data Curation, Writing - Review & Editing
Pamela Cohn: Formal Analysis, Supervision, Investigation, Writing – Original Draft, Review and Editing
Matthew Metzler: Methodology, Investigation
Marissa Huynh: Methodology, Investigation
Arsalan Mirjafari: Writing – Review and Editing, Formal Analysis, Investigation
Patrick C. Hillesheim: Conceptualization, Methodology, Validation, Resources, Visualization, Formal Analysis, Supervision, Project Administration, Writing – Original Draft, Review & Editing, Funding acquisition

ORCID:

Patrick C. Hillesheim: 0000-0002-9567-4002
Pamela Cohn: 0000-0002-3346-6128
Matthias Zeller: 0000-0002-3305-852X
Arsalan Mirjafari: 0000-0002-5502-0602

References

(1) MacFarlane, D. R.; Kar, M.; Pringle, J. M. *Fundamentals of Ionic Liquids*; Wiley-VCH Verlag GmbH & Co. KGaA: Weinheim, Germany, 2017. https://doi.org/10.1002/9783527340033.

(2) Welton, T. Ionic Liquids: A Brief History. *Biophys. Rev.* **2018**, *10* (3), 691–706. https://doi.org/10.1007/s12551-018-0419-2.

(3) Deetlefs, M.; Fanselow, M.; Seddon, K. R. Ionic Liquids: The View from Mount Improbable. *RSC Adv.* **2016**, *6* (6), 4280–4288. https://doi.org/10.1039/C5RA05829E.

(4) Hayes, R.; Warr, G. G.; Atkin, R. Structure and Nanostructure in Ionic Liquids. *Chem. Rev.* **2015**, *115* (13), 6357–6426. https://doi.org/10.1021/cr500411q.

(5) Philippi, F.; Welton, T. Targeted Modifications in Ionic Liquids – from Understanding to Design. *Phys. Chem. Chem. Phys.* **2021**, *23* (12), 6993–7021. https://doi.org/10.1039/D1CP00216C.

(6) Silva, W.; Zanatta, M.; Ferreira, A. S.; Corvo, M. C.; Cabrita, E. J. Revisiting Ionic Liquid Structure-Property Relationship: A Critical Analysis. *Int. J. Mol. Sci.* **2020**, *21* (20), 7745. https://doi.org/10.3390/ijms21207745.

(7) Yu, G.; Zhao, D.; Wen, L.; Yang, S.; Chen, X. Viscosity of Ionic Liquids: Database, Observation, and Quantitative Structure-Property Relationship Analysis. *AIChE J.* **2012**, *58* (9), 2885–2899. https://doi.org/10.1002/aic.12786.

(8) Binnemans, K. Ionic Liquid Crystals. *Chem. Rev.* **2005**, *105* (11), 4148–4204. https://doi.org/10.1021/cr0400919.

(9) Wang, X.; Sternberg, M.; Kohler, F. T. U.; Melcher, B. U.; Wasserscheid, P.; Meyer, K. Long-Alkyl-Chain-Derivatized Imidazolium Salts and Ionic Liquid Crystals with Tailor-Made Properties. *RSC Adv* **2014**, *4* (24), 12476–12481. https://doi.org/10.1039/C3RA47250G.

(10) Yao, W.; Wang, H.; Cui, G.; Li, Z.; Zhu, A.; Zhang, S.; Wang, J. Tuning the Hydrophilicity and Hydrophobicity of the Respective Cation and Anion: Reversible Phase Transfer of Ionic Liquids. *Angew. Chem. Int. Ed.* **2016**, *55* (28), 7934–7938. https://doi.org/10.1002/anie.201600419.

(11) Zhou, F.; Liang, Y.; Liu, W. Ionic Liquid Lubricants: Designed Chemistry for Engineering Applications. *Chem. Soc. Rev.* **2009**, *38* (9), 2590. https://doi.org/10.1039/b817899m.

(12) El Seoud, O. A.; Keppeler, N.; Malek, N. I.; Galgano, P. D. Ionic Liquid-Based Surfactants: Recent Advances in Their Syntheses, Solution Properties, and Applications. *Polymers* **2021**, *13* (7), 1100. https://doi.org/10.3390/polym13071100.

(13) Egorova, K. S.; Gordeev, E. G.; Ananikov, V. P. Biological Activity of Ionic Liquids and Their Application in Pharmaceutics and Medicine. *Chem. Rev.* **2017**, *117* (10), 7132–7189. https://doi.org/10.1021/acs.chemrev.6b00562.

(14) Bergamo, V. Z.; Donato, R. K.; Dalla Lana, D. F.; Donato, K. J. Z.; Ortega, G. G.; Schrekker, H. S.; Fuentefria, A. M. Imidazolium Salts as Antifungal Agents: Strong Antibiofilm Activity against Multidrug-Resistant *Candida Tropicalis* Isolates. *Lett. Appl. Microbiol.* **2015**, *60* (1), 66–71. https://doi.org/10.1111/lam.12338.

(15) Rębiś, T.; Niemczak, M.; Płócienniczak, P.; Pernak, J.; Milczarek, G. Voltammetric Sensor Based on Long Alkyl Chain Tetraalkylammonium Ionic Liquids Comprising Ascorbate Anion for Determination of Nitrite. *Microchim. Acta* **2021**, *188* (2), 54. https://doi.org/10.1007/s00604-021-04713-4.

(16) Xue, L.; Gurung, E.; Tamas, G.; Koh, Y. P.; Shadeck, M.; Simon, S. L.; Maroncelli, M.; Quitevis, E. L. Effect of Alkyl Chain Branching on Physicochemical Properties of Imidazolium-Based Ionic Liquids. *J. Chem. Eng. Data* **2016**, *61* (3), 1078–1091. https://doi.org/10.1021/acs.jced.5b00658.

(17) Rabideau, B. D.; Soltani, M.; Parker, R. A.; Siu, B.; Salter, E. A.; Wierzbicki, A.; West, K. N.; Davis, J. H. Tuning the Melting Point of Selected Ionic Liquids through Adjustment of the Cation's Dipole Moment. *Phys. Chem. Chem. Phys.* **2020**, *22* (21), 12301–12311. https://doi.org/10.1039/D0CP01214A.

(18) Siegel, D. J.; Anderson, G. I.; Paul, L. M.; Seibert, P. J.; Hillesheim, P. C.; Sheng, Y.; Zeller, M.; Taubert, A.; Werner, P.; Balischewski, C.; Michael, S. F.; Mirjafari, A. Design Principles of Lipid-like Ionic Liquids for Gene Delivery. *ACS Appl. Bio Mater.* **2021**, *4* (6), 4737–4743. https://doi.org/10.1021/acsabm.1c00252.

(19) Henderson, W. A.; Young, Jr., V. G.; Fox, D. M.; De Long, H. C.; Trulove, P. C. Alkyl vs. Alkoxy Chains on Ionic Liquid Cations. *Chem Commun* **2006**, No. 35, 3708–3710. https://doi.org/10.1039/B606381K.

(20) Canongia Lopes, J. N. A.; Pádua, A. A. H. Nanostructural Organization in Ionic Liquids. *J. Phys. Chem. B* **2006**, *110* (7), 3330–3335. https://doi.org/10.1021/jp056006y.

(21) Dupont, J. On the Solid, Liquid and Solution Structural Organization of Imidazolium Ionic Liquids. *J. Braz. Chem. Soc.* **2004**, *15* (3), 341–350. https://doi.org/10.1590/S0103-50532004000300002.

(22) Wang, Y.; Parvis, F.; Hossain, Md. I.; Ma, K.; Jarošová, R.; Swain, G. M.; Blanchard, G. J. Local and Long-Range Organization in Room Temperature Ionic Liquids. *Langmuir* **2021**, *37* (2), 605–615. https://doi.org/10.1021/acs.langmuir.9b03995.
(23) Winterton, N. Crystallography of Ionic Liquids. In *Ionic Liquids Completely UnCOILed*; John Wiley & Sons, Ltd, 2015; pp 231–534. https://doi.org/10.1002/9781118840061.ch11.
(24) Dean, P. M.; Pringle, J. M.; Forsyth, C. M.; Scott, J. L.; MacFarlane, D. R. Interactions in Bisamide Ionic Liquids—Insights from a Hirshfeld Surface Analysis of Their Crystalline States. *New J. Chem.* **2008**, *32* (12), 2121. https://doi.org/10.1039/b809606f.
(25) Dean, P. M.; Pringle, J. M.; MacFarlane, D. R. Structural Analysis of Low Melting Organic Salts: Perspectives on Ionic Liquids. *Phys. Chem. Chem. Phys.* **2010**, *12* (32), 9144. https://doi.org/10.1039/c003519j.
(26) Zeng, Q.; Mukherjee, A.; Müller, P.; Rogers, R. D.; Myerson, A. S. Exploring the Role of Ionic Liquids to Tune the Polymorphic Outcome of Organic Compounds. *Chem. Sci.* **2018**, *9* (6), 1510–1520. https://doi.org/10.1039/C7SC04353H.
(27) Nishikawa, K.; Wang, S.; Endo, T.; Tozaki, K. Melting and Crystallization Behaviors of an Ionic Liquid, 1-Isopropyl-3-Methylimidazolium Bromide, Studied by Using Nanowatt-Stabilized Differential Scanning Calorimetry. *Bull. Chem. Soc. Jpn.* **2009**, *82* (7), 806–812. https://doi.org/10.1246/bcsj.82.806.
(28) Bradley, A. E.; Hardacre, C.; Holbrey, J. D.; Johnston, S.; McMath, S. E. J.; Nieuwenhuyzen, M. Small-Angle X-Ray Scattering Studies of Liquid Crystalline 1-Alkyl-3-Methylimidazolium Salts. *Chem. Mater.* **2002**, *14* (2), 629–635. https://doi.org/10.1021/cm010542v.
(29) Downard, A.; Earle, M. J.; Hardacre, C.; McMath, S. E. J.; Nieuwenhuyzen, M.; Teat, S. J. Structural Studies of Crystalline 1-Alkyl-3-Methylimidazolium Chloride Salts. *Chem. Mater.* **2004**, *16* (1), 43–48. https://doi.org/10.1021/cm034344a.
(30) Getsis, A.; Mudring, A.-V. 1-Dodecyl-3-Methylimidazolium Bromide Monohydrate. *Acta Crystallogr. Sect. E Struct. Rep. Online* **2005**, *61* (9), o2945–o2946. https://doi.org/10.1107/S1600536805025717.
(31) Guillet, E.; Imbert, D.; Scopelliti, R.; Bünzli, J.-C. G. Tuning the Emission Color of Europium-Containing Ionic Liquid-Crystalline Phases. *Chem. Mater.* **2004**, *16* (21), 4063–4070. https://doi.org/10.1021/cm049296o.
(32) Getsis, A.; Mudring, A.-V. Imidazolium Based Ionic Liquid Crystals: Structure, Photophysical and Thermal Behaviour of [C_n Mim]Br·xH_2O (n = 12, 14; X=0, 1). *Cryst. Res. Technol.* **2008**, *43* (11), 1187–1196. https://doi.org/10.1002/crat.200800345.
(33) Zhao, Y.; Hu, X.; Zhang, Q.; Guan, P. Crystal Structure and Aggregation Behavior in Water of Ionic Liquid 1-Hexadecyl-3-Methylimidazolium Bromide. *Mater. Lett.* **2010**, *64* (7), 794–797. https://doi.org/10.1016/j.matlet.2010.01.007.
(34) Saouane, S.; Fabbiani, F. P. A. Structural Behavior of Long-Chain Imidazolium-Based Ionic Liquid [C_{10} Mim]Cl–Water Mixtures. *Cryst. Growth Des.* **2015**, *15* (8), 3875–3884. https://doi.org/10.1021/acs.cgd.5b00494.
(35) Groom, C. R.; Allen, F. H. The Cambridge Structural Database in Retrospect and Prospect. *Angew. Chem. Int. Ed.* **2014**, *53* (3), 662–671. https://doi.org/10.1002/anie.201306438.
(36) Groom, C. R.; Bruno, I. J.; Lightfoot, M. P.; Ward, S. C. The Cambridge Structural Database. *Acta Crystallogr. Sect. B Struct. Sci. Cryst. Eng. Mater.* **2016**, *72* (2), 171–179. https://doi.org/10.1107/S2052520616003954.
(37) Ding, X.; Shen, N.; Li, J.; Huang, X. Transition Metal-Containing Ionic Liquid Crystals with 1-Decyl-2,3-dimethylimidazolium: Facile Syntheses, Crystal Structures, Thermal Properties and NH_3 Detection. *ChemistrySelect* **2018**, *3* (13), 3731–3736. https://doi.org/10.1002/slct.201800470.
(38) Renier, O.; Bousrez, G.; Yang, M.; Hölter, M.; Mallick, B.; Smetana, V.; Mudring, A.-V. Developing Design Tools for Introducing and Tuning Structural Order in Ionic Liquids. *CrystEngComm* **2021**, *23* (8), 1785–1795. https://doi.org/10.1039/D0CE01672A.
(39) Deetlefs, M.; Hardacre, C.; Nieuwenhuyzen, M.; Sheppard, O.; Soper, A. K. Structure of Ionic Liquid−Benzene Mixtures. *J. Phys. Chem. B* **2005**, *109* (4), 1593–1598. https://doi.org/10.1021/jp047742p.
(40) Wang, Y.; Voth, G. A. Tail Aggregation and Domain Diffusion in Ionic Liquids. *J. Phys. Chem. B* **2006**, *110* (37), 18601–18608. https://doi.org/10.1021/jp063199w.
(41) Balevicius, V.; Gdaniec, Z.; Aidas, K.; Tamuliene, J. NMR and Quantum Chemistry Study of Mesoscopic Effects in Ionic Liquids. *J. Phys. Chem. A* **2010**, *114* (16), 5365–5371. https://doi.org/10.1021/jp909293b.
(42) Würthner, F.; Wortmann, R.; Meerholz, K. Chromophore Design for Photorefractive Organic Materials. *ChemPhysChem* **2002**, *3* (1), 17–31. https://doi.org/10.1002/1439-7641(20020118)3:1<17::AID-CPHC17>3.0.CO;2-N.

(43) Bonhôte, P.; Dias, A.-P.; Papageorgiou, N.; Kalyanasundaram, K.; Grätzel, M. Hydrophobic, Highly Conductive Ambient-Temperature Molten Salts. *Inorg. Chem.* **1996**, *35* (5), 1168–1178. https://doi.org/10.1021/ic951325x.

(44) Wang, Y.-L.; Li, B.; Sarman, S.; Mocci, F.; Lu, Z.-Y.; Yuan, J.; Laaksonen, A.; Fayer, M. D. Microstructural and Dynamical Heterogeneities in Ionic Liquids. *Chem. Rev.* **2020**, *120* (13), 5798–5877. https://doi.org/10.1021/acs.chemrev.9b00693.

(45) Spackman, M. A.; Jayatilaka, D. Hirshfeld Surface Analysis. *CrystEngComm* **2009**, *11* (1), 19–32. https://doi.org/10.1039/B818330A.

(46) Apex3 V2019.1-0, SAINT V8.40A, 2019.

(47) Krause, L.; Herbst-Irmer, R.; Sheldrick, G. M.; Stalke, D. Comparison of Silver and Molybdenum Microfocus X-Ray Sources for Single-Crystal Structure Determination. *J. Appl. Crystallogr.* **2015**, *48* (1), 3–10. https://doi.org/10.1107/S1600576714022985.

(48) SHELXTL Suite of Programs, Version 6.14, 2000-2003, Bruker Advanced X-Ray Solutions.

(49) Sheldrick, G. M. A Short History of *SHELX*. *Acta Crystallogr. A* **2008**, *64* (1), 112–122. https://doi.org/10.1107/S0108767307043930.

(50) Sheldrick, G. M. *SHELXT* – Integrated Space-Group and Crystal-Structure Determination. *Acta Crystallogr. Sect. Found. Adv.* **2015**, *71* (1), 3–8. https://doi.org/10.1107/S2053273314026370.

(51) Sheldrick, G. M. Crystal Structure Refinement with *SHELXL*. *Acta Crystallogr. Sect. C Struct. Chem.* **2015**, *71* (1), 3–8. https://doi.org/10.1107/S2053229614024218.

(52) Dolomanov, O. V.; Bourhis, L. J.; Gildea, R. J.; Howard, J. A. K.; Puschmann, H. *OLEX2* : A Complete Structure Solution, Refinement and Analysis Program. *J. Appl. Crystallogr.* **2009**, *42* (2), 339–341. https://doi.org/10.1107/S0021889808042726.

(53) Hübschle, C. B.; Sheldrick, G. M.; Dittrich, B. *ShelXle* : A Qt Graphical User Interface for *SHELXL*. *J. Appl. Crystallogr.* **2011**, *44* (6), 1281–1284. https://doi.org/10.1107/S0021889811043202.

(54) Cooper, R. I.; Gould, R. O.; Parsons, S.; Watkin, D. J. The Derivation of Non-Merohedral Twin Laws during Refinement by Analysis of Poorly Fitting Intensity Data and the Refinement of Non-Merohedrally Twinned Crystal Structures in the Program CRYSTALS. *J. Appl. Crystallogr.* **2002**, *35* (2), 168–174. https://doi.org/10.1107/S0021889802000249.

(55) Farrugia, L. J. *WinGX* and *ORTEP for Windows* : An Update. *J. Appl. Crystallogr.* **2012**, *45* (4), 849–854. https://doi.org/10.1107/S0021889812029111.

(56) 2twin: Multiple Independent Twinning in ShelXL. Copyright 2017, Daniel W. Paley.

(57) Spackman, P. R.; Turner, M. J.; McKinnon, J. J.; Wolff, S. K.; Grimwood, D. J.; Jayatilaka, D.; Spackman, M. A. *CrystalExplorer* : A Program for Hirshfeld Surface Analysis, Visualization and Quantitative Analysis of Molecular Crystals. *J. Appl. Crystallogr.* **2021**, *54* (3), 1006–1011. https://doi.org/10.1107/S1600576721002910.

(58) Macrae, C. F.; Bruno, I. J.; Chisholm, J. A.; Edgington, P. R.; McCabe, P.; Pidcock, E.; Rodriguez-Monge, L.; Taylor, R.; van de Streek, J.; Wood, P. A. *Mercury CSD 2.0* – New Features for the Visualization and Investigation of Crystal Structures. *J. Appl. Crystallogr.* **2008**, *41* (2), 466–470. https://doi.org/10.1107/S0021889807067908.

(59) Yang, M.; Mallick, B.; Mudring, A.-V. On the Mesophase Formation of 1,3-Dialkylimidazolium Ionic Liquids. *Cryst. Growth Des.* **2013**, *13* (7), 3068–3077. https://doi.org/10.1021/cg4004593.

(60) De Roche, J.; Gordon, C. M.; Imrie, C. T.; Ingram, M. D.; Kennedy, A. R.; Lo Celso, F.; Triolo, A. Application of Complementary Experimental Techniques to Characterization of the Phase Behavior of [C_{16}Mim][PF_6] and [C_{14}Mim][PF_6]. *Chem. Mater.* **2003**, *15* (16), 3089–3097. https://doi.org/10.1021/cm021378u.

(61) López-Martin, I.; Burello, E.; Davey, P. N.; Seddon, K. R.; Rothenberg, G. Anion and Cation Effects on Imidazolium Salt Melting Points: A Descriptor Modelling Study. *ChemPhysChem* **2007**, *8* (5), 690–695. https://doi.org/10.1002/cphc.200600637.

(62) Xu, F.; Matsumoto, K.; Hagiwara, R. Effects of Alkyl Chain Length and Anion Size on Thermal and Structural Properties for 1-Alkyl-3-Methylimidazolium Hexafluorocomplex Salts (CxMImAF6, x = 14, 16 and 18; A = P, As, Sb, Nb and Ta). *Dalton Trans.* **2012**, *41* (12), 3494. https://doi.org/10.1039/c2dt11693f.

(63) Gordon, C. M.; Holbrey, J. D.; Kennedy, A. R.; Seddon, K. R. Ionic Liquid Crystals: Hexafluorophosphate Salts. *J. Mater. Chem.* **1998**, *8* (12), 2627–2636. https://doi.org/10.1039/a806169f.

(64) Gavezzotti, A. The Lines-of-Force Landscape of Interactions between Molecules in Crystals; Cohesive *versus* Tolerant and `collateral Damage' Contact. *Acta Crystallogr. B* **2010**, *66* (3), 396–406. https://doi.org/10.1107/S0108768110008074.

(65) Spackman, M. A.; McKinnon, J. J. Fingerprinting Intermolecular Interactions in Molecular Crystals. *CrystEngComm* **2002**, *4* (66), 378–392. https://doi.org/10.1039/B203191B.
(66) McGaughey, G. B.; Gagné, M.; Rappé, A. K. π-Stacking Interactions. *J. Biol. Chem.* **1998**, *273* (25), 15458–15463. https://doi.org/10.1074/jbc.273.25.15458.
(67) Martinez, C. R.; Iverson, B. L. Rethinking the Term "Pi-Stacking." *Chem. Sci.* **2012**, *3* (7), 2191. https://doi.org/10.1039/c2sc20045g.
(68) Gao, W.; Tian, Y.; Xuan, X. How the Cation–Cation π–π Stacking Occurs: A Theoretical Investigation into Ionic Clusters of Imidazolium. *J. Mol. Graph. Model.* **2015**, *60*, 118–123. https://doi.org/10.1016/j.jmgm.2015.04.002.
(69) García-Saiz, A.; de Pedro, I.; Migowski, P.; Vallcorba, O.; Junquera, J.; Blanco, J. A.; Fabelo, O.; Sheptyakov, D.; Waerenborgh, J. C.; Fernández-Díaz, M. T.; Rius, J.; Dupont, J.; Gonzalez, J. A.; Fernández, J. R. Anion−π and Halide–Halide Nonbonding Interactions in a New Ionic Liquid Based on Imidazolium Cation with Three-Dimensional Magnetic Ordering in the Solid State. *Inorg. Chem.* **2014**, *53* (16), 8384–8396. https://doi.org/10.1021/ic500882z.
(70) Pandey, D. K.; Materny, A.; Kiefer, J.; Singh, D. K. Quantification of the Interactions in Halide-Anion-Based Imidazolium Ionic Liquids. *J. Ion. Liq.* **2022**, *2* (2), 100032. https://doi.org/10.1016/j.jil.2022.100032.
(71) Beichel, W.; Yu, Y.; Dlubek, G.; Krause-Rehberg, R.; Pionteck, J.; Pfefferkorn, D.; Bulut, S.; Bejan, D.; Friedrich, C.; Krossing, I. Free Volume in Ionic Liquids: A Connection of Experimentally Accessible Observables from PALS and PVT Experiments with the Molecular Structure from XRD Data. *Phys. Chem. Chem. Phys.* **2013**, *15* (22), 8821. https://doi.org/10.1039/c3cp43306d.
(72) Dlubek, G.; Yu, Y.; Krause-Rehberg, R.; Beichel, W.; Bulut, S.; Pogodina, N.; Krossing, I.; Friedrich, Ch. Free Volume in Imidazolium Triflimide ([C3MIM][NTf2]) Ionic Liquid from Positron Lifetime: Amorphous, Crystalline, and Liquid States. *J. Chem. Phys.* **2010**, *133* (12), 124502. https://doi.org/10.1063/1.3487522.
(73) Fayer, M. D. Dynamics and Structure of Room Temperature Ionic Liquids. *Chem. Phys. Lett.* **2014**, *616–617*, 259–274. https://doi.org/10.1016/j.cplett.2014.09.062.
(74) Abbott, A. P. Application of Hole Theory to the Viscosity of Ionic and Molecular Liquids. *ChemPhysChem* **2004**, *5* (8), 1242–1246. https://doi.org/10.1002/cphc.200400190.
(75) Turner, M. J.; McKinnon, J. J.; Jayatilaka, D.; Spackman, M. A. Visualisation and Characterisation of Voids in Crystalline Materials. *CrystEngComm* **2011**, *13* (6), 1804–1813. https://doi.org/10.1039/C0CE00683A.
(76) Philippi, F.; Rauber, D.; Palumbo, O.; Goloviznina, K.; McDaniel, J.; Pugh, D.; Suarez, S.; Fraenza, C. C.; Padua, A.; Kay, C. W. M.; Welton, T. Flexibility Is the Key to Tuning the Transport Properties of Fluorinated Imide-Based Ionic Liquids. *Chem. Sci.* **2022**, 10.1039.D2SC03074H. https://doi.org/10.1039/D2SC03074H.
(77) Fredlake, C. P.; Crosthwaite, J. M.; Hert, D. G.; Aki, S. N. V. K.; Brennecke, J. F. Thermophysical Properties of Imidazolium-Based Ionic Liquids. *J. Chem. Eng. Data* **2004**, *49* (4), 954–964. https://doi.org/10.1021/je034261a.
(78) *Ionic Liquids: Physicochemical Properties*, 1st ed.; Zhang, S., Ed.; Elsevier: Amsterdam, The Netherlands ; Boston ; London, 2009.
(79) Kroon, M. C.; Buijs, W.; Peters, C. J.; Witkamp, G.-J. Quantum Chemical Aided Prediction of the Thermal Decomposition Mechanisms and Temperatures of Ionic Liquids. *Thermochim. Acta* **2007**, *465* (1), 40–47. https://doi.org/10.1016/j.tca.2007.09.003.
(80) Maton, C.; De Vos, N.; Stevens, C. V. Ionic Liquid Thermal Stabilities: Decomposition Mechanisms and Analysis Tools. *Chem Soc Rev* **2013**, *42* (13), 5963–5977. https://doi.org/10.1039/C3CS60071H.
(81) Shimizu, Y.; Ohte, Y.; Yamamura, Y.; Saito, K. Effects of Thermal History on Thermal Anomaly in Solid of Ionic Liquid Compound, [C_4Mim][Tf_2N]. *Chem. Lett.* **2007**, *36* (12), 1484–1485. https://doi.org/10.1246/cl.2007.1484.
(82) Mudring, A.-V. Solidification of Ionic Liquids: Theory and Techniques. *Aust. J. Chem.* **2010**, *63* (4), 544. https://doi.org/10.1071/CH10017.
(83) Nozaki, Y.; Yamaguchi, K.; Tomida, K.; Taniguchi, N.; Hara, H.; Takikawa, Y.; Sadakane, K.; Nakamura, K.; Konishi, T.; Fukao, K. Phase Transition and Dynamics in Imidazolium-Based Ionic Liquid Crystals through a Metastable Highly Ordered Smectic Phase. *J. Phys. Chem. B* **2016**, *120* (23), 5291–5300. https://doi.org/10.1021/acs.jpcb.6b03804.
(84) Yang, M.; Mallick, B.; Mudring, A.-V. A Systematic Study on the Mesomorphic Behavior of Asymmetrical 1-Alkyl-3-Dodecylimidazolium Bromides. *Cryst. Growth Des.* **2014**, *14* (4), 1561–1571. https://doi.org/10.1021/cg401396n.
(85) Howe, D.; Wilson, J.; Rosokha, S. V. Solvent and Ionic Atmosphere Effects in Anion−π Interactions: Complexes of Halide Anions with p-Benzoquinones. *J. Phys. Chem. A* **2022**, *126* (26), 4255–4263. https://doi.org/10.1021/acs.jpca.2c03491.

(86) Rather, M. A.; Rather, G. M.; Pandit, S. A.; Bhat, S. A.; Bhat, M. A. Determination of Cmc of Imidazolium Based Surface Active Ionic Liquids through Probe-Less UV–Vis Spectrophotometry. *Talanta* **2015**, *131*, 55–58. https://doi.org/10.1016/j.talanta.2014.07.046.

(87) Billeci, F.; D'Anna, F.; Chiarotto, I.; Feroci, M.; Marullo, S. The Anion Impact on the Self-Assembly of Naphthalene Diimide Diimidazolium Salts. *New J Chem* **2017**, *41* (22), 13889–13901. https://doi.org/10.1039/C7NJ03705H.

Table 1: Table summarizing important dihedral angles which affect alkyl chain orientation in the cations of the crystal structures. All four disordered cations in the asymmetric unit of **4** are included (A – D).

	2	**3**	**4 (A)**	**4 (B)**	**4 (C)**	**4 (D)**
ALKYL-CORE PLANE ANGLE	92.93(10) °	153.3(10) °	145.5(5) °	143.8(4) °	166.3(6) °	168.0(6) °
C2—N3—C8—C9	74.7(5) °	107.0(2) °	116.4(15) °	108.0(12) °	13.0(4) °	92.6(17) °
N3—C8—C9—C10	60.6(5) °	174.1(17) °	165.8(10) °	162.0(9) °	179.5(15) °	156.6(12) °
C8—C9—C10—C11	178.5(4) °	60.0(3) °	168.8(10) °	163.7(9) °	171.6(13) °	96.0(16) °

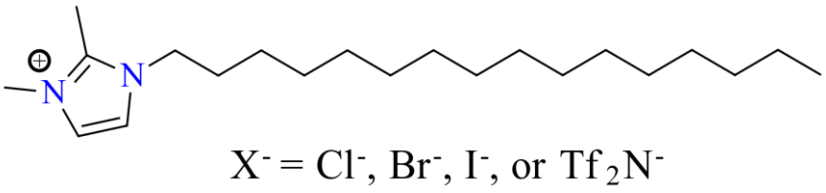

Figure 1. Depiction of the IL systems examined herein.

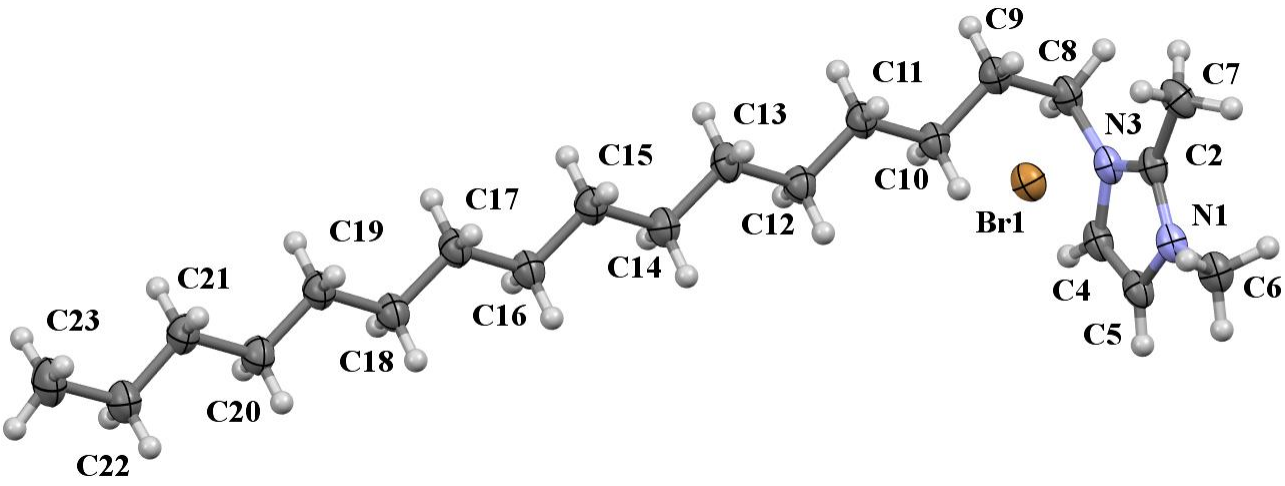

Figure 2. Asymmetric unit of **2** shown with 50% probability ellipsoids. Gray = carbon, white = hydrogen, blue = nitrogen, tan = bromine.

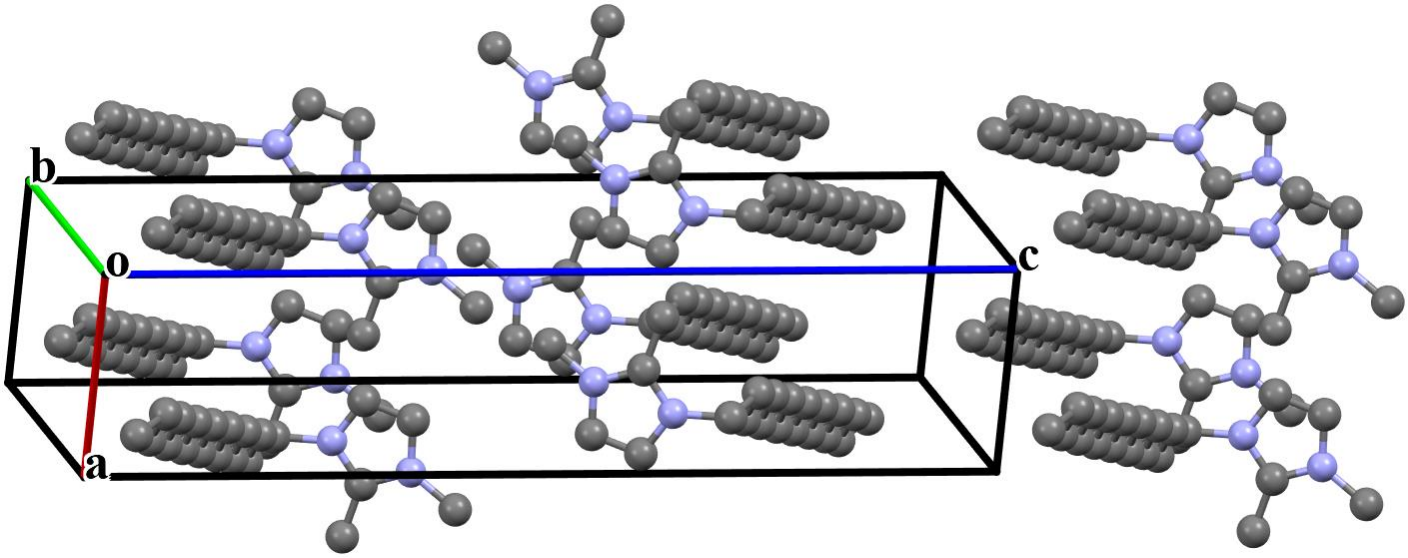

Figure 3. Representative packing diagram for the cations of compound **2** showing the alternating alignment of the alkyl groups. Hydrogens and bromide atoms are omitted for clarity.

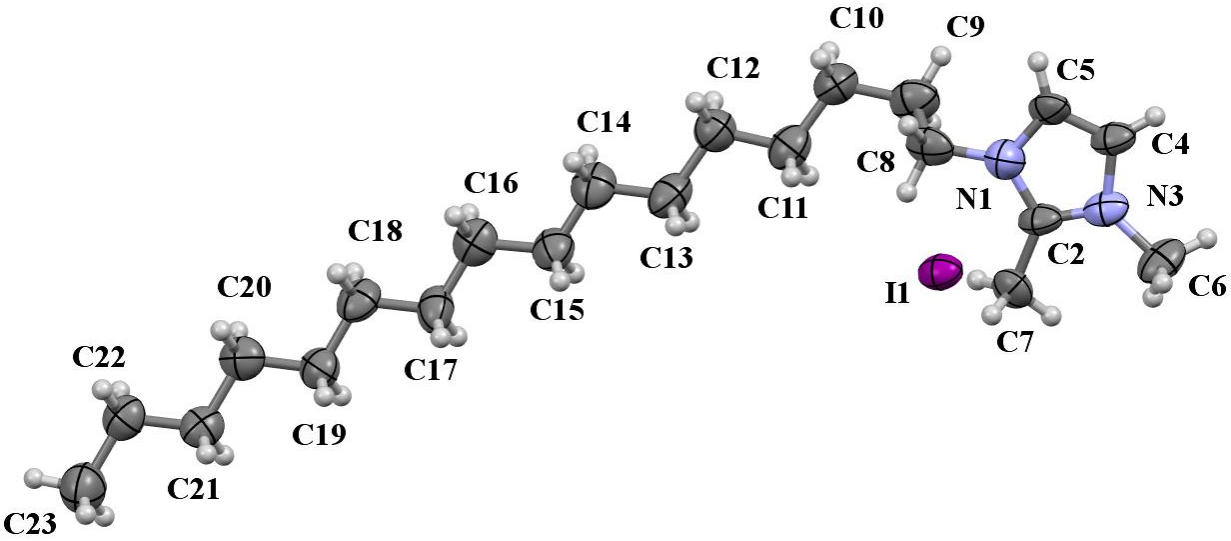

Figure 4. Asymmetric unit of **3** shown with 50% probability ellipsoids. Gray = carbon, white = hydrogen, blue = nitrogen, purple = iodine.

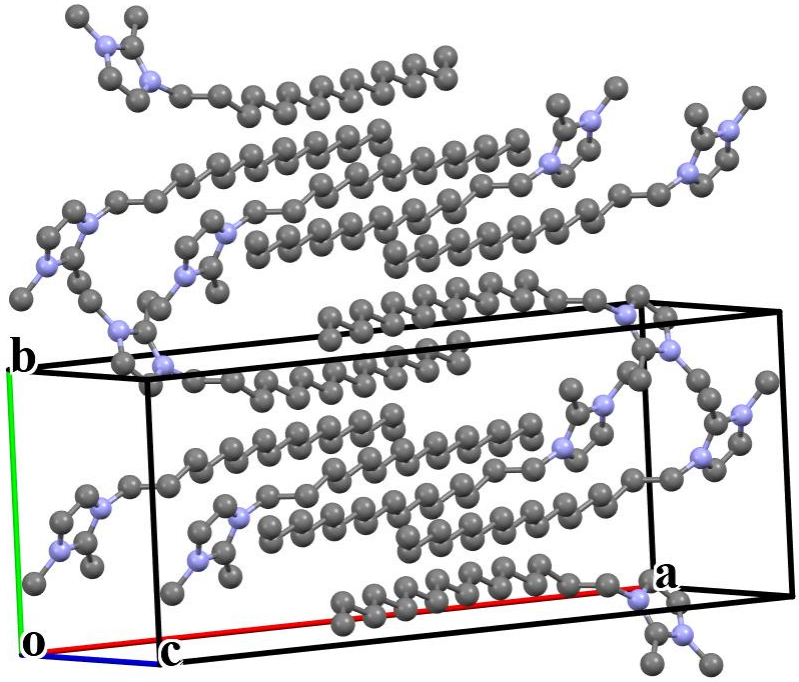

Figure 5. Representative packing diagram for the cations of compound **3** showing the interdigitated alkyl groups. Hydrogens and iodide atoms are omitted for clarity.

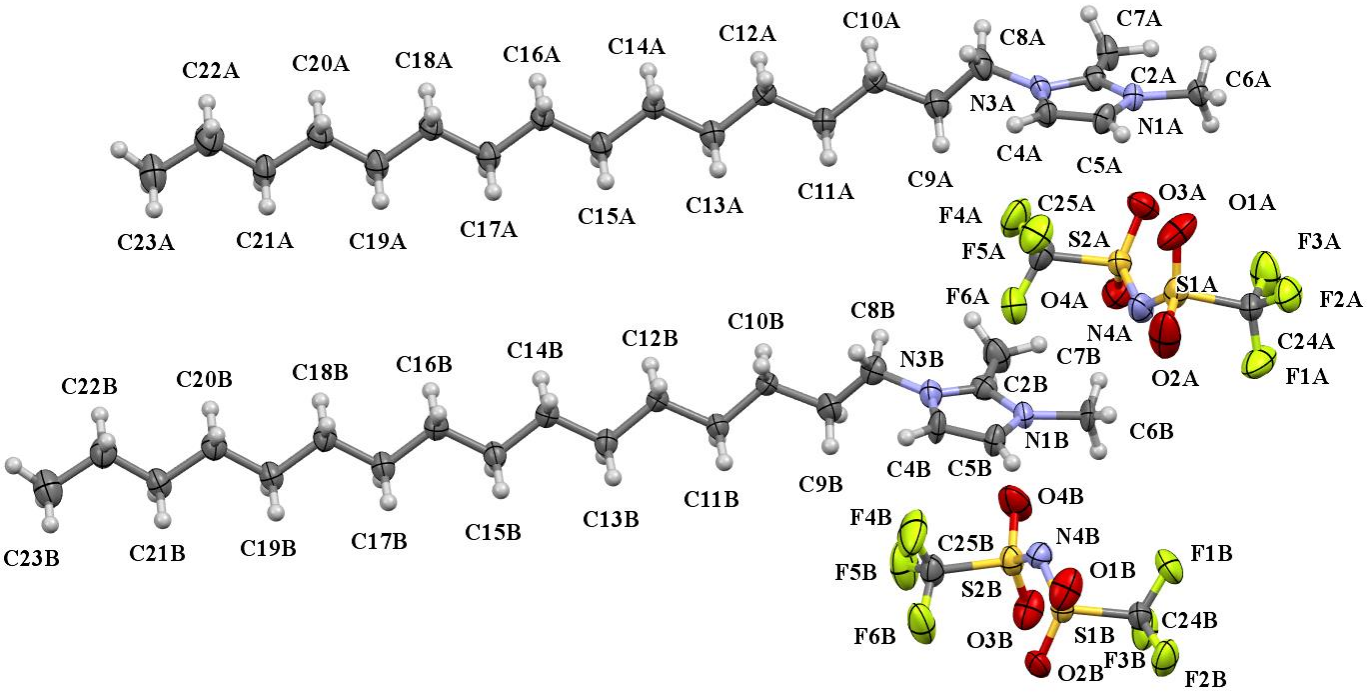

Figure 6. Asymmetric unit of **4** shown with 50% probability ellipsoids. Disordered parts C and D omitted for clarity. Gray = carbon, white = hydrogen, blue = nitrogen, red = oxygen, green = fluorine, yellow = sulfur.

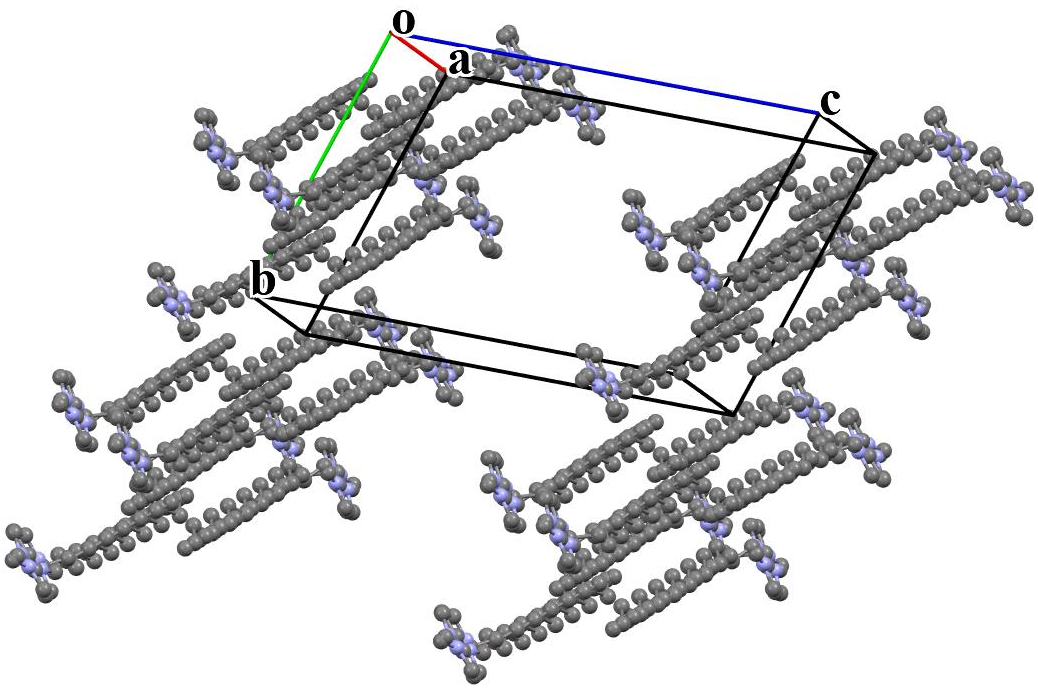

Figure 7. Representative packing diagram for the cations in compound **4** showing the interdigitated alkyl groups. Hydrogen atoms, Tf_2N^- anions are omitted for clarity. Both disordered portions of the cations are shown.

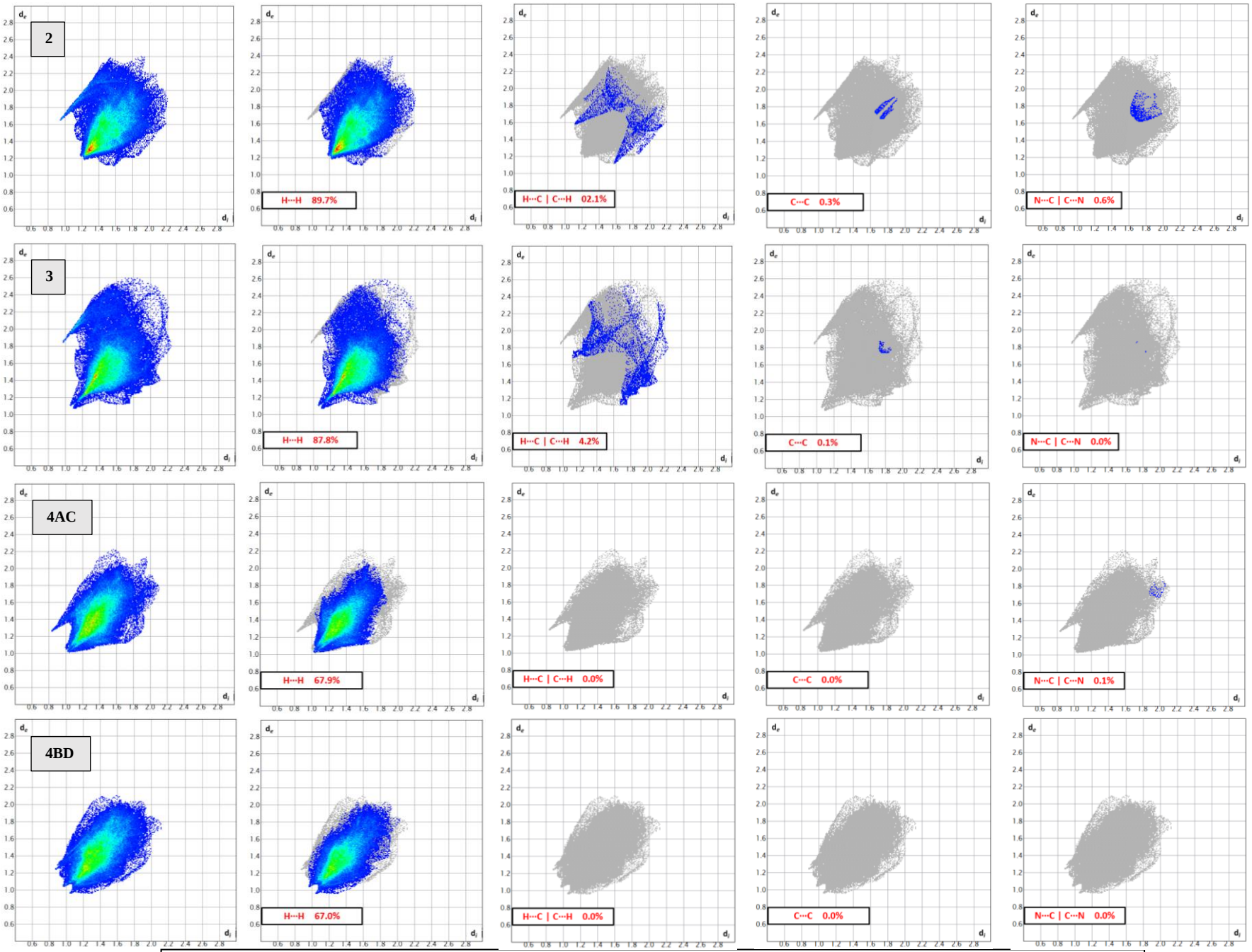

Figure 8. Fingerprints for compounds **2 - 4** showing important intermolecular interactions of the cations.

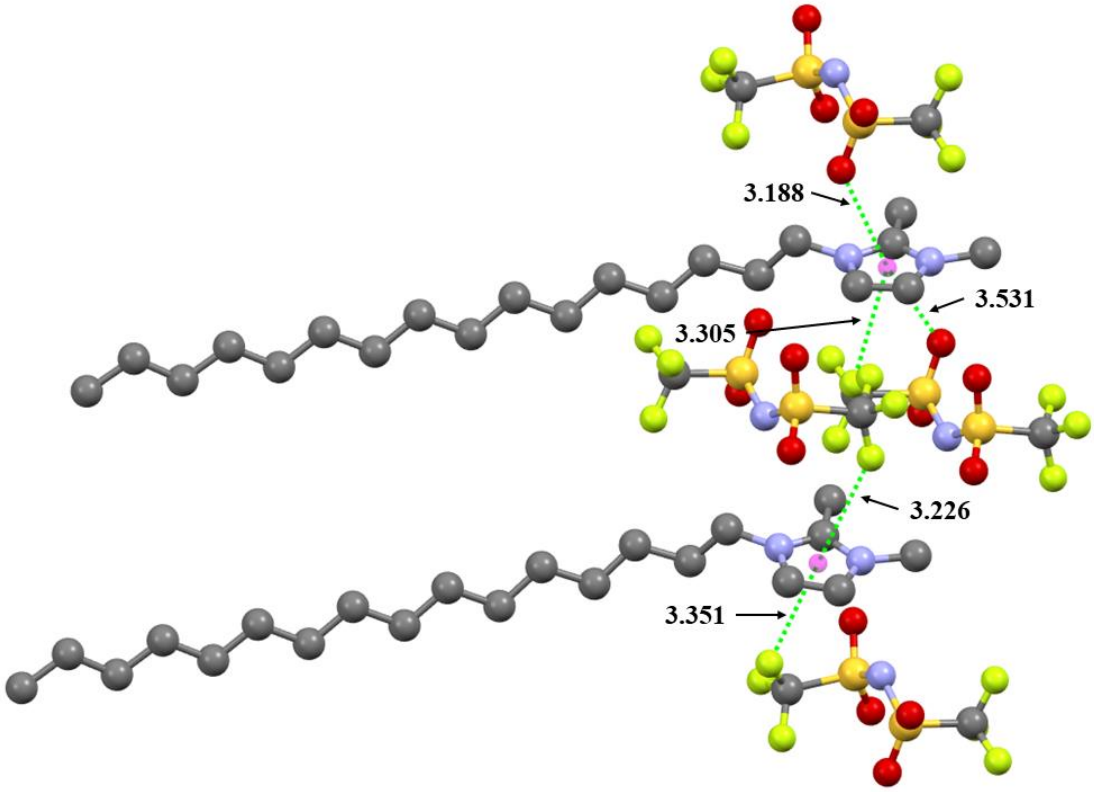

Figure 9. Depiction of anion···π interactions in **4**. Hydrogens and disorder are omitted for clarity. Distances are shown in angstroms to the centroid of the rings.

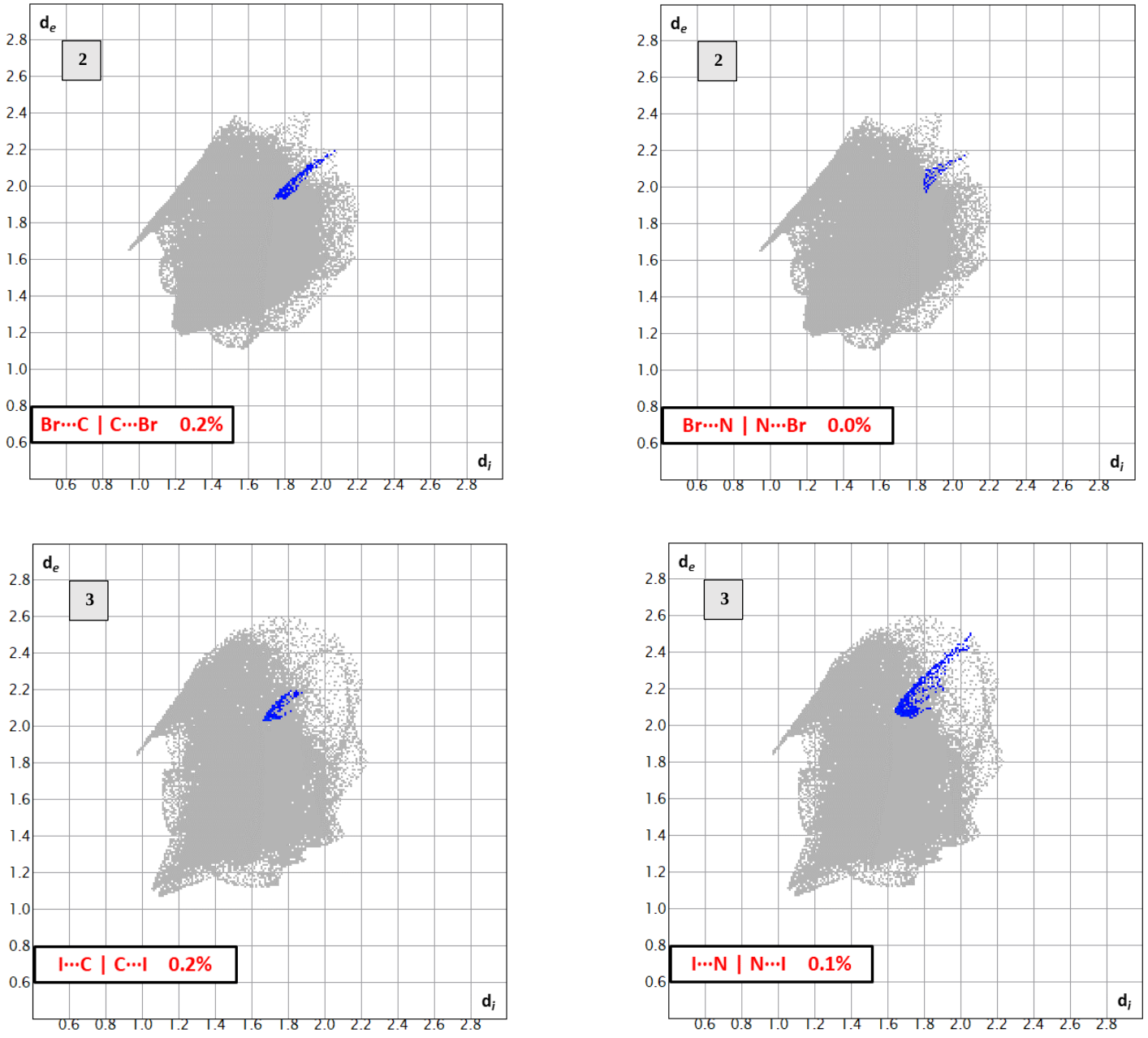

Figure 10. Fingerprints for **2** and **3** showing the negligible anion···π interactions in the crystals.

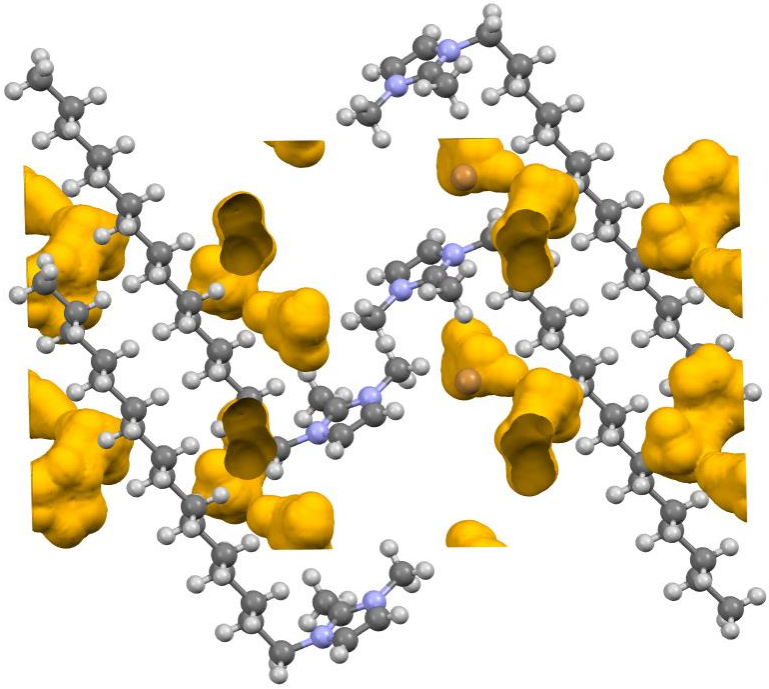

Figure 11. Depiction of void spaces (yellow) in the structure of **2**.

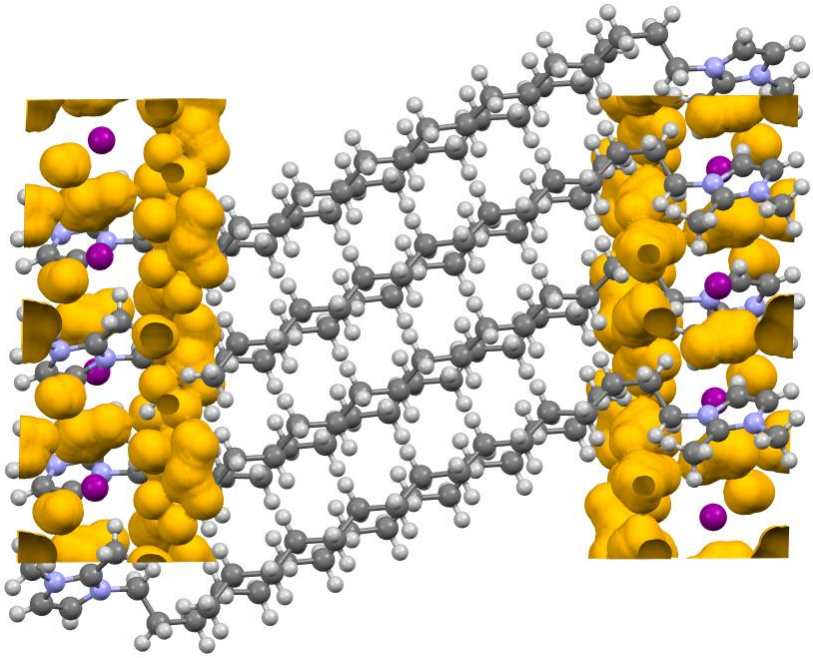

Figure 12. Depiction of void spaces (yellow) in the structure of **3**.

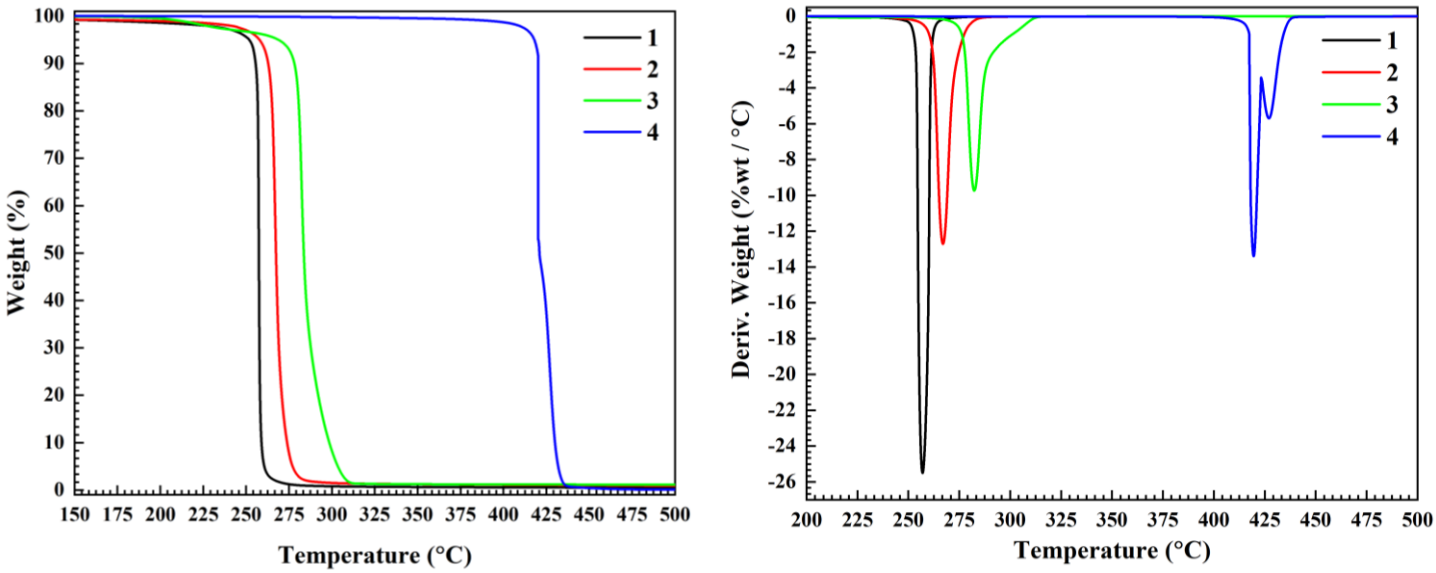

Figure 13. Thermal decomposition traces for compounds **1** – **4** (left) and the derivative curves (right).

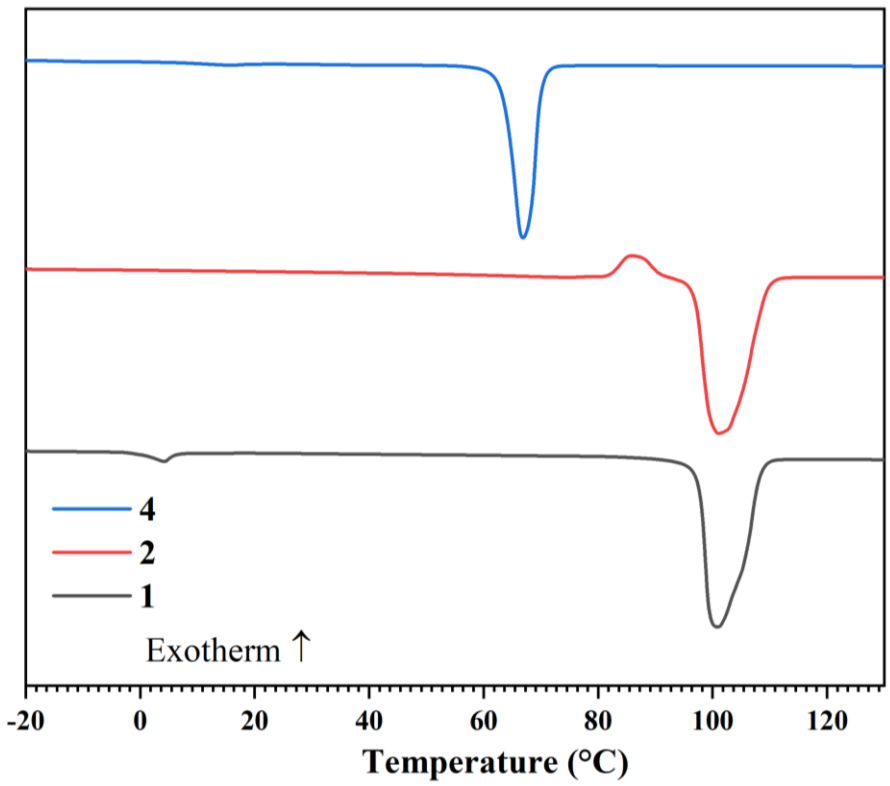

Figure 14. DSC traces for compounds **1**, **2**, and **4** taken from the 2nd heating cycle for each compound. Y axis is offset for clarity.

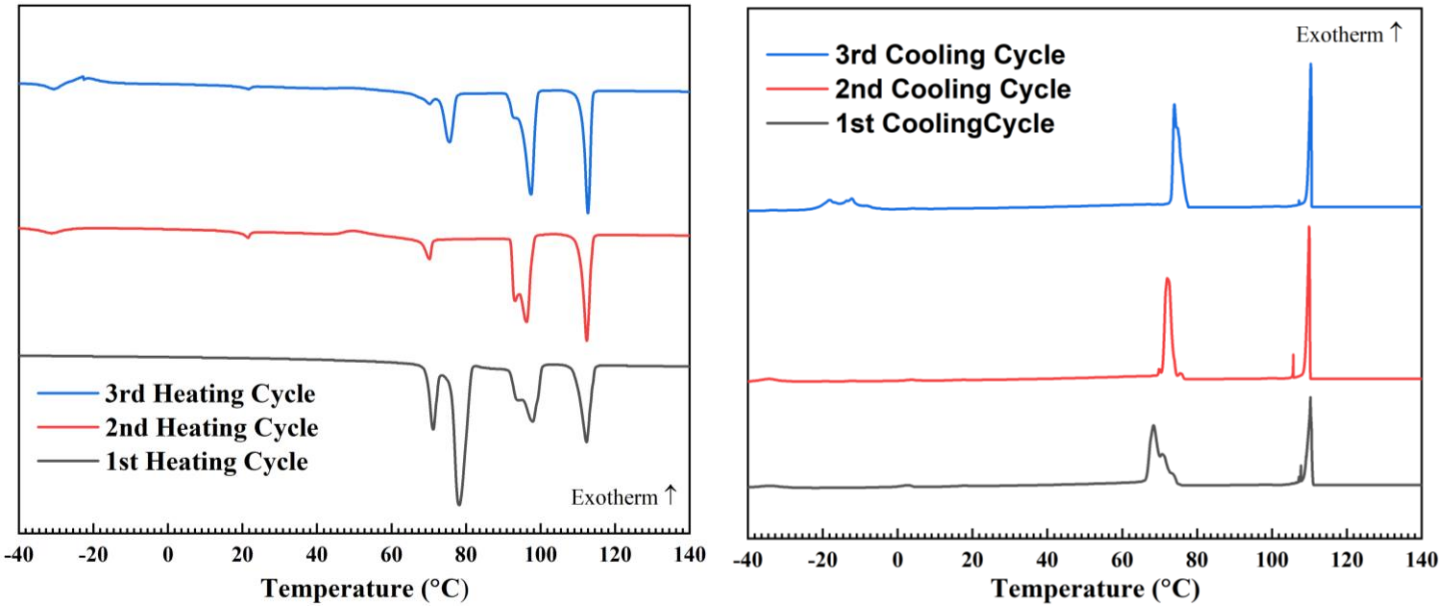

Figure 15. Traces of the three consecutive heating cycles (left) and cooling (right) for compound **3**. Y axis is offset for clarity.

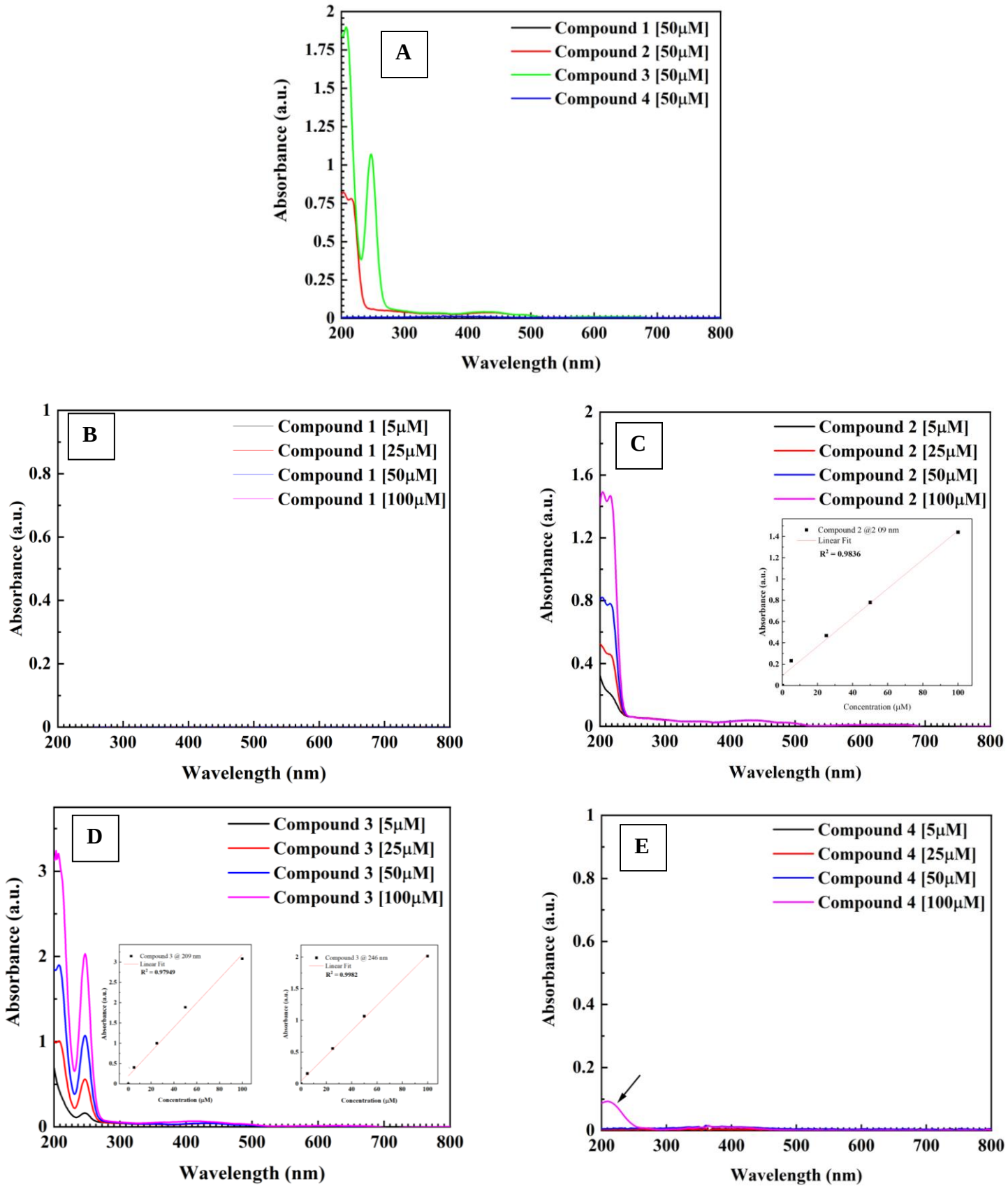

Figure 16. (A) UV-*vis* spectra for compounds **1** – **4** at 50 μM concentration in acetonitrile. **(B – E)** UV-*vis* concentration studies for compounds **1** – **4** in acetonitrile.

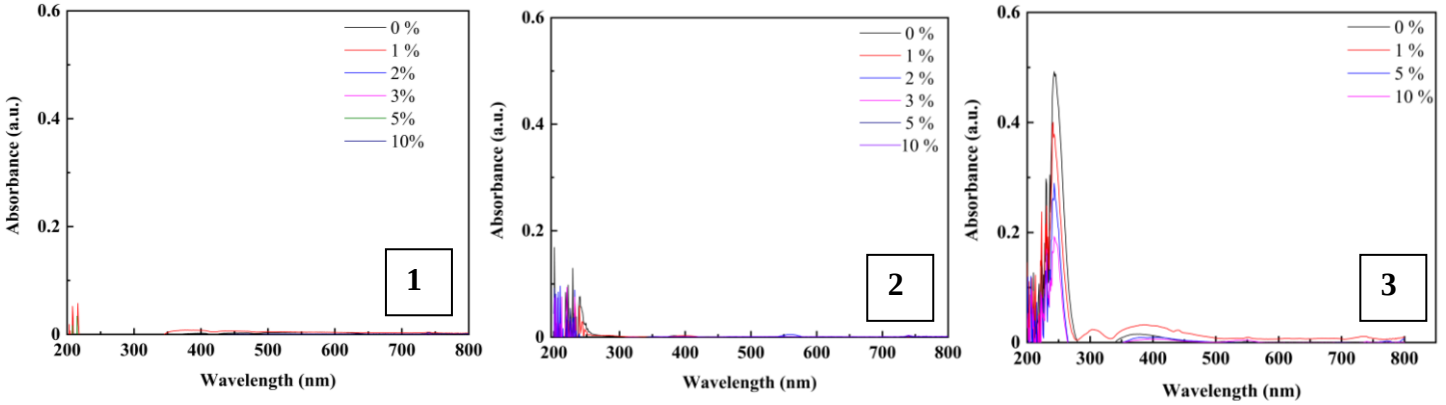

Figure 17. UV-*vis* spectra of compounds **1 – 3** in mixtures of methanol : chloroform. Percentages refer to methanol.